TECHNICAL REPORT STANDARD TITLE PAGE

1. Report No. 109300-5-F	2. Government Accession No.	3. Recipient's Catalog No.
4. Title and Subtitle: REMOTE SENSING STUDIES IN THE NEW YORK BIGHT		5. Report Date: July 1975 6. Performing Organization Code
7. Author(s): C. T. Wezernak, D. R. Lyzenga, and F. C. Polcyn		8. Performing Organization Report No. 109300-5-F
9. Performing Organization Name and Address: Environmental Research Institute of Michigan, Infrared and Optics Division, P. O. Box 618, Ann Arbor, Michigan 48107		10. Work Unit No. 11. Contract or Grant No. 04-4-158-33
12. Sponsoring Agency Name and Address: National Oceanographic and Atmospheric Administration, National Environmental Satellite Service, Washington, D. C.		13. Type of Report and Period Covered: Final Technical Report 14. Sponsoring Agency Code

15. Supplementary Notes

Dr. D. K. Clark was Technical Monitor of this project.

16. Abstract

Multispectral remote sensing data were collected in the New York Bight during the morning and afternoon of 7 April 1973. The morning mission was coincident with the ERTS-1 pass over the study area. Data were processed to show surface temperature, surface chlorophyll, and Secchi disc transparency. A limited amount of ERTS-1 processing was performed to show the suspended solids distribution in the adjacent bay areas. Additional data products document ocean dumping practices and show the movement of water masses as evidenced by dye tracer materials.

17. Key Words	18. Distribution Statement
Remote sensing New York Bight Surface circulation Water quality Ocean dumping MESA	Initial distribution is indicated at the end of this document.

19. Security Classif. (of this report)	20. Security Classif. (of this page)	21. No. of Pages	22. Price
Unclassified	Unclassified	76	

PREFACE

This report is submitted by the Environmental Research Institute of Michigan in fulfillment of NOAA Grant 04-4-158-33 under the sponsorship of the National Oceanic and Atmospheric Administration. Technical Monitor for the project was D. K. Clark. Principal Investigator was F. C. Polcyn.

Several individuals at ERIM contributed to the project. In particular the contributions of P. Hasell, J. Tone, and J. McKimmy are acknowledged with sincere thanks. Mr. Hasell directed airborne collection; whereas Ms. Tone and Ms. McKimmy assisted in the data processing.

CONTENTS

FIGURES

FIGURES (Continued)

TABLES

REMOTE SENSING STUDY IN THE NEW YORK BIGHT

1

INTRODUCTION

Described in the sections which follow are the results of a remote sensing program of data collection and analysis undertaken under the sponsorship of the National Oceanic and Atmospheric Administration, National Environmental Satellite Service (NOAA/NESS), Spacecraft Oceanography group, in the New York Bight. The program was conducted in support of one phase of the NOAA Marine Ecosystems Analysis (MESA) Program in the Bight. Successful aircraft multispectral missions were carried out by the Environmental Research Institute of Michigan (ERIM) on 7 April 1973. The morning mission on that date coincided with the ERTS-1 satellite pass over the area.

The principal objectives of the remote sensing program were to provide data, which when combined with shipboard measurements, would describe the surface waters of the area and their general circulation. Specifically the remote sensing program was designed to provide the following information:

1. sea surface temperature distribution
2. surface chlorophyll concentrations
3. secchi disc transparency
4. document ocean dumping practices
5. movement of water masses as evidenced by dye tracer materials

2

STUDY AREA

The coastal waters adjacent to the New York Metropolitan Region are being subjected to extreme cultural pressures. The area is the repository for substantial quantities of sewage sludge, industrial acid-waste, construction debris, and dredge spoils. The designated dumping areas are shown in Fig. 1.

Sewage sludge is normally disposed of at a location approximately 19 km. south of Long Island. At the present time, approximately 9,500 cu. m. per day are dumped at this location. In addition to nutrient enrichment of the overlying waters, the introduction of heavy metals, etc. at the immediate dump location, the practice often results in the formation of extensive surface films.

Acid-iron wastes are normally disposed of at a location approximately 20 km. east of New Jersey and 24 km. south of Long Island. The waste solution contains approximately 8% H_2SO_4, 10% $FeSO_4$, and small quantities of various metallic elements. The wastes are dispersed by barge over a hairpin-shaped course of approximately 10 km. in length. The subsequent oxidation of the iron from the ferrous to the ferric state produces a suspension which tends to remain in a distinct pattern for long periods after dispersal.

In addition to the above substances, dredging spoils from the New York metropolitan harbor area and construction debris are dumped in the New York Bight.

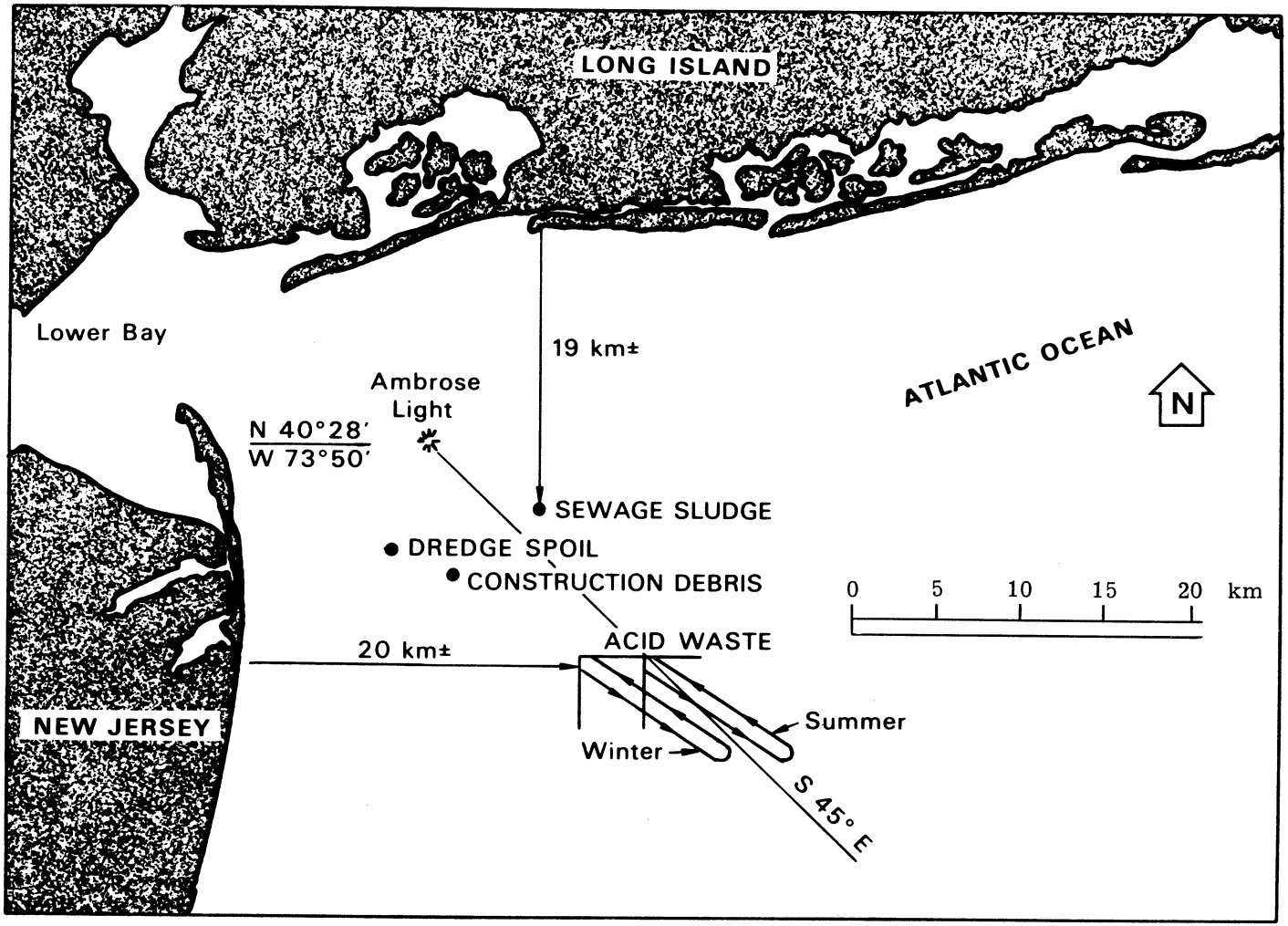

FIGURE 1. WASTE DISPOSAL SITES IN THE NEW YORK BIGHT

3

METHODS

Low-altitude aircraft remote sensing data were collected using the ERIM multispectral scanner. A description of the multispectral sensor system and data processing procedures used (for both aircraft and satellite data) is presented in the sections which follow. An intensive ground truth data collection and analysis program was conducted by the NOAA/NESS Spacecraft Oceanography group. Described in the sections which follow are the methods used to acquire supplementary data.

3.1 AIRCRAFT DATA COLLECTION

The ERIM M-7 multispectral scanner was used for remote sensing data collection [1]. Use of this instrument permits simultaneous data collection in twelve narrow spectral bands over a wavelength range from 0.32 to 11.7 μm. The system includes a spectrometer for dispersing the radiation spectrally and filtered detector arrays placed at the focal points of a double-ended optical-mechanical scanner. Additional detector positions are used for spectral bands in the ultraviolet and the infrared.

Signals from the detectors are recorded on magnetic tape for later image reconstruction and data processing. As an integral feature of the system, reference lamps, an input proportional to the sun energy, and adjustable temperature reference plates are viewed each revolution of the scanner mirror. The basic configuration of the scanner is shown in Fig. 2.

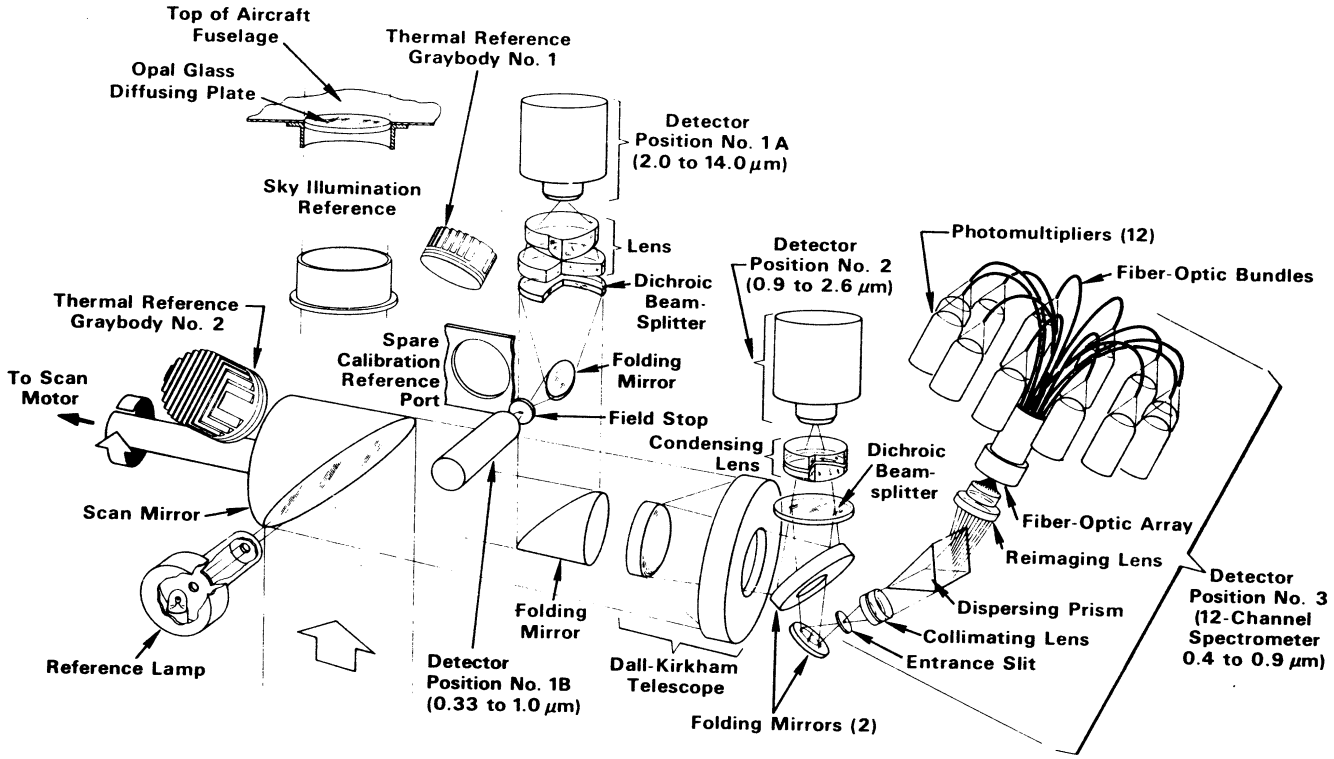

FIGURE 2. SCHEMATIC OF ERIM MULTISPECTRAL SCANNER, M7

The scanner is positioned in the aircraft so as to provide continuous scanning perpendicular to the flight line as shown in Fig. 3. As the aircraft advances, the rotating mirror scans the scene over a 90° field of view, in a regular manner so that a continuous presentation is built up line by line. In addition to data collected by the multispectral scanner, photographic data are normally collected along the flight track. In this particular program, black-white and color photographic records were obtained.

Aircraft data were collected from an altitude of 3,048 meters on 7 April 1973 during two stages of the tidal cycle. The morning overflight commenced at 0830 EST and was completed at 1043 EST. The afternoon data collection began at 1341 EST and was completed at 1544 EST. The area over which data were collected during each overflight is shown in Fig. 4.

3.2 GROUND TRUTH DATA COLLECTION AND ANALYSIS

As indicated above, ground truth data collection and analysis was conducted by NOAA/NESS. Partial results from this intensive field program were reported by Clark and co-workers [2].

In addition to the above, a limited data collection and analysis program was carried out by ERIM. Parameters measured included temperature, pH, turbidity, suspended solids, total solids, salinity, chlorophyll *a*, PO_4-P, total Fe, and Secchi disk transparency. Analyses were performed in accordance with the procedures outlined in Standard Methods [3] and Biological and Laboratory Methods [4]. *In situ* determinations included transparency, salinity, and temperature. All other analyses were performed using laboratory procedures.

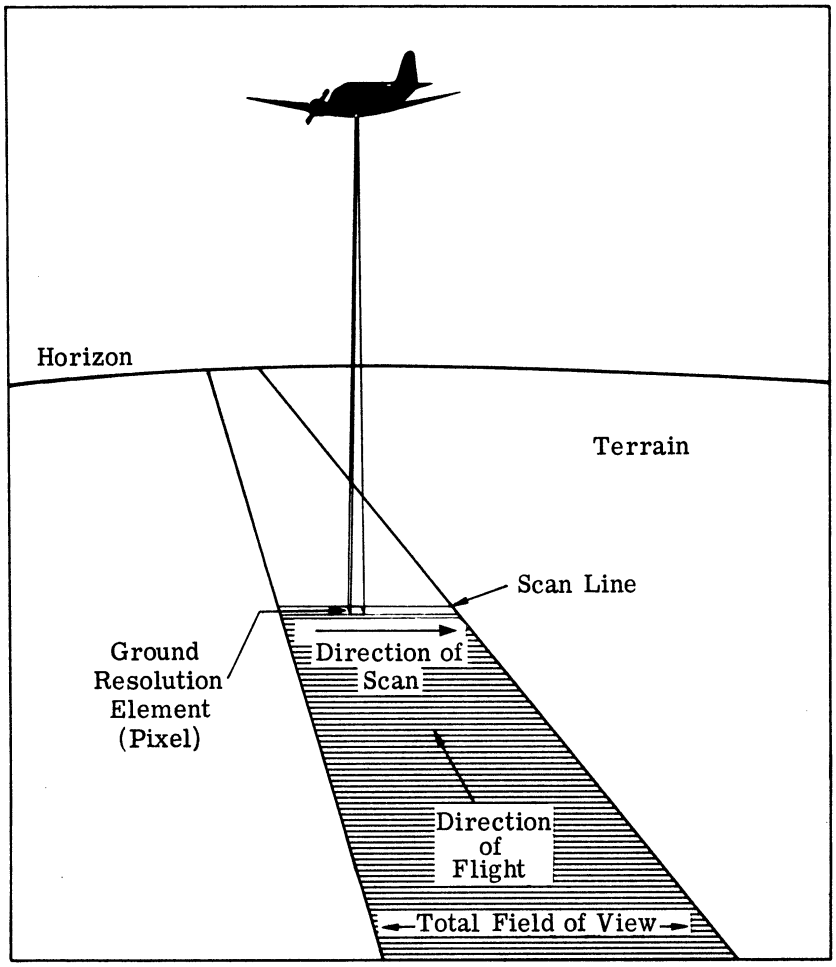

FIGURE 3. AIRBORNE DATA COLLECTION

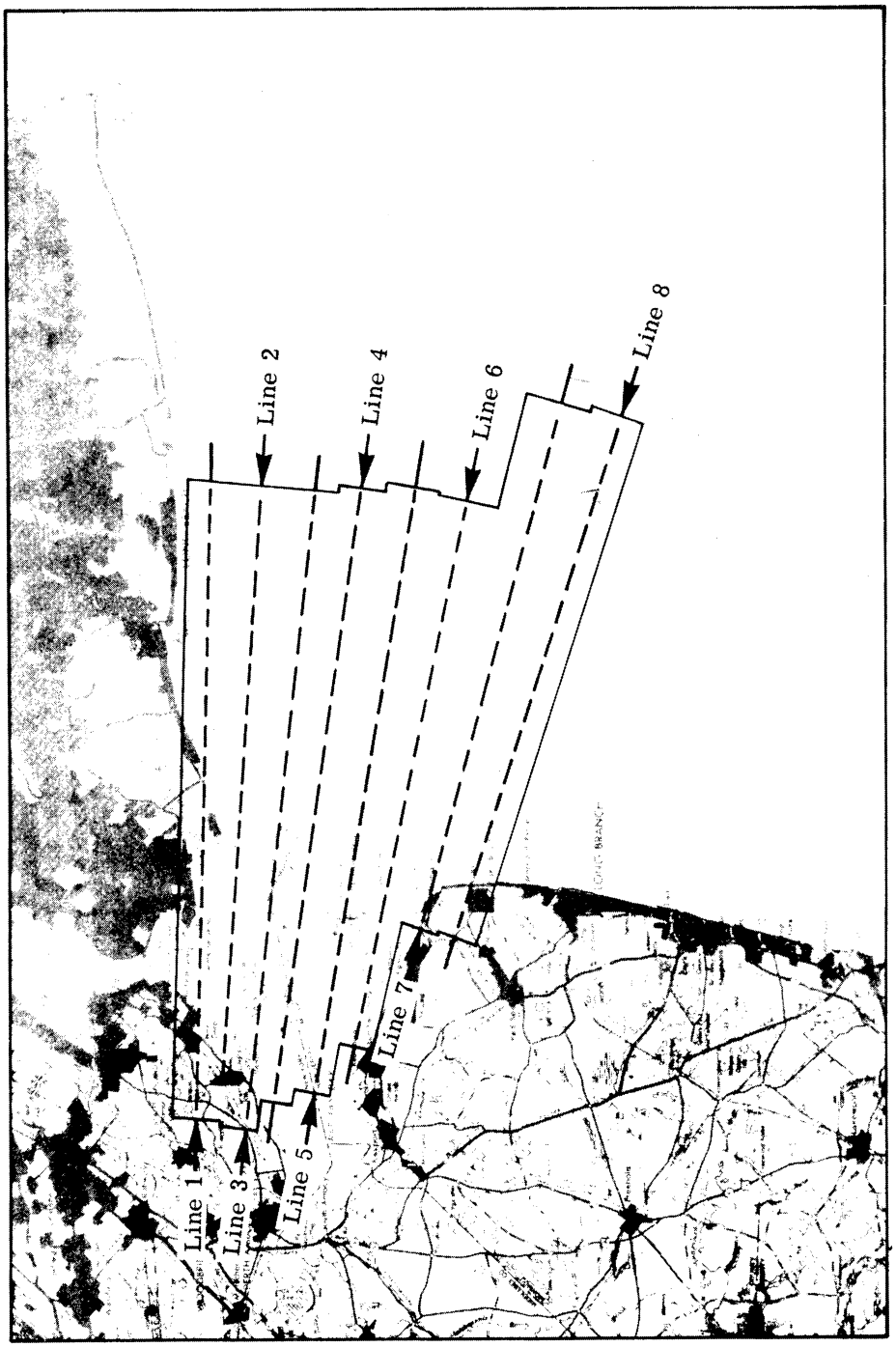

FIGURE 4. MISSION DATA AREA COVERAGE, 7 APRIL 1973

Chlorophyll *a* determinations were performed using the Trichromatic Method. Turbidity measurements were made using the Hach 2100 A turbidimeter. Suspended solids determinations, defined as "total non-filtrable residue", were performed using the Standard Methods procedure [3]. A standard 50 cm. oceanographic Secchi disk was used for transparency measurement.

3.3 PROCESSING OF ERTS-1 DATA

Processing of ERTS-1 data, as part of this program, was restricted to a limited analysis of portions of frame E-1258-15082 collected 7 April 1973.

The data obtained in the ERTS-1 program was applied to the study of the problems described through computer processing using ERTS-1 computer compatible tapes (CCT).

The data supplied by NASA were collected by the ERTS-1 multispectral scanner (MSS) from an altitude of approximately 915 km. in the following spectral bands:

SPECTRAL BAND	WAVELENGTH (μm)
4	0.5-0.6
5	0.6-0.7
6	0.7-0.8
7	0.8-1.1

The area of each resolution element was approximately 0.45 hectares. The information in bands 4, 5, and 6 was recorded with a 7-bit resolution (127 grey levels); and in band 7 with a 6-bit resolution (64 grey levels). Since the system was not optimized for data collection over water, the total information content for water areas was generally limited to a few grey levels.

The processing of ERTS data recorded on CCT's included density level slicing of individual spectral bands, and statistical analysis of selected target areas. Grey maps and color-coded digital displays were produced as required. De-striping and smoothing of the CCT data was applied on two occasions to produce maps free of the characteristic ERTS stripes caused by detector non-uniformity.

The general processing procedure included: (1) reformatting of the data onto a 7-track digital tape, (2) preparation of working grey maps, and (3) production of line-prints through selected target areas. Based on an analysis of line-print data, integer levels for the production of final digital products were established. Spectral band 7 was used to edit-out land areas. Statistical data for selected target areas were generated using standard ERIM statistical programs. The STAT program determines signatures of specified training sets of MSS data, and optionally prints histograms and/or statistical information about each field.

Smoothing of the data to produce maps free of the characteristic ERTS-1 stripes was accomplished using a program (WINDOW) written by D. Lyzenga of ERIM. WINDOW is a sliding-rectangle smoothing program designed to average data values over an arbitrary size rectangle of points. The output tape has the same number of lines and points as the input tape, however, each output data value is the average of nLxmP input data values. In this case smoothing was applied using a 6 x 6 resolution element rectangle.

3.4 PROCESSING OF AIRCRAFT DATA AND ATMOSPHERIC EFFECTS

Aircraft multispectral scanner data were converted from analog to digital format for subsequent machine processing. Because of strong winds at the

3048 meter altitude, large discrepancies between ground-speeds on the eastbound and westbound runs were noted. These effects were largely compensated for in the normal smoothing operation, with the result that correct aspect ratios were achieved. Standard ERIM programs for correcting the data for scan angle effects were included in the preprocessing steps.

Atmospheric corrections for the 9.3-11.7 μm spectral band were calculated using MODRAD [5]. The New York Bight atmosphere was modelled for temperature and moisture characteristics from radiosonde data taken at Fort Totten, New York. Temperature corrections for the ERIM thermal data (3048 meters, 9.3-11.7 μm) were as follows:

ZENITH ANGLE	°C
180	1.83
157.5	1.98
135	2.50

Calculations for atmospheric effects in the visible region of the spectrum were made using the radiative transfer model developed by Turner and co-workers [6, 7, 8]. The path reflectances resulting from path radiance effects for an altitude of 3048 meters, solar zenith angle of 54°, visibility of 23 km., were as follows:

λ	ρ_p
0.45 μm	0.058
0.52 μm	0.037
0.65 μm	0.020

4

THEORETICAL AND PRACTICAL CONSIDERATIONS IN THE USE OF REMOTE SENSING FOR TEMPERATURE, CHLOROPHYLL, AND TRANSPARENCY MEASUREMENT

4.1 PRINCIPLES OF THERMAL REMOTE SENSING

Remote sensing techniques for temperature measurement are based on the fact that all substances above absolute zero (0°K) emit electromagnetic energy. The radiant emittance of a perfect radiator or blackbody is described by Planck's law:

$$L_\lambda = 2\pi c^2 h\lambda^{-5} \left[\left(e^{hc/\lambda kT} \right) - 1 \right]^{-1}$$

where L = radiance at wavelength

c = speed of light

h = Planck's constant

λ = wavelength

T = absolute temperature

k = Stefan-Boltzmann constant

The above expression applies to a perfect blackbody, i.e., an object that absorbs all radiation. Since few objects even approximate a perfect blackbody, the factor ε (emissivity) is introduced. Blackbodies have an emissivity of 1, whereas other objects have an emissivity less than 1 which varies with wavelength. Hence the equation for a greybody is written

$$L_\lambda^g = (2\pi c^2 h)\, \varepsilon_\lambda \lambda^{-5} \left[\left(e^{hc/\lambda kT} \right) - 1 \right]^{-1}$$

Substituting

$$c_1 = 2\pi c^2 h$$

$$c_2 = \frac{hc}{k}$$

$$L_\lambda^g = \frac{c_1 \varepsilon_\lambda}{\lambda^5 \left[\left(e^{c_2/\lambda T}\right) - 1\right]}$$

Therefore, Planck's law indicates that the radiation emitted by an object is a function of the object's absolute temperature and the wavelength of observation. However, before the above relationship is utilized for radiometric measurements from aircraft altitudes, several factors must be considered including selection of the operating spectral band. A region of the electromagnetic spectrum must be selected where the water emissivity and atmospheric transmission are high.

The distribution of emitted energy over a broad wavelength band is temperature dependent. The position of the peak of radiant emittance is defined by Wien's Displacement Law:

$$\lambda max = \frac{2898\ \mu°K}{T}$$

From this relationship, it is evident that the wavelength (λ) of the energy peak decreases as the temperature (T) is increased. These relationships are illustrated for a blackbody in Figure 5. Therefore, for most earth-bound objects (roughly 300°K), the radiation peak occurs at approximately 10 μm. Atmospheric attenuation at this wavelength is not a serious problem. A good "atmospheric window" exists in this region, as shown in Figure 6.

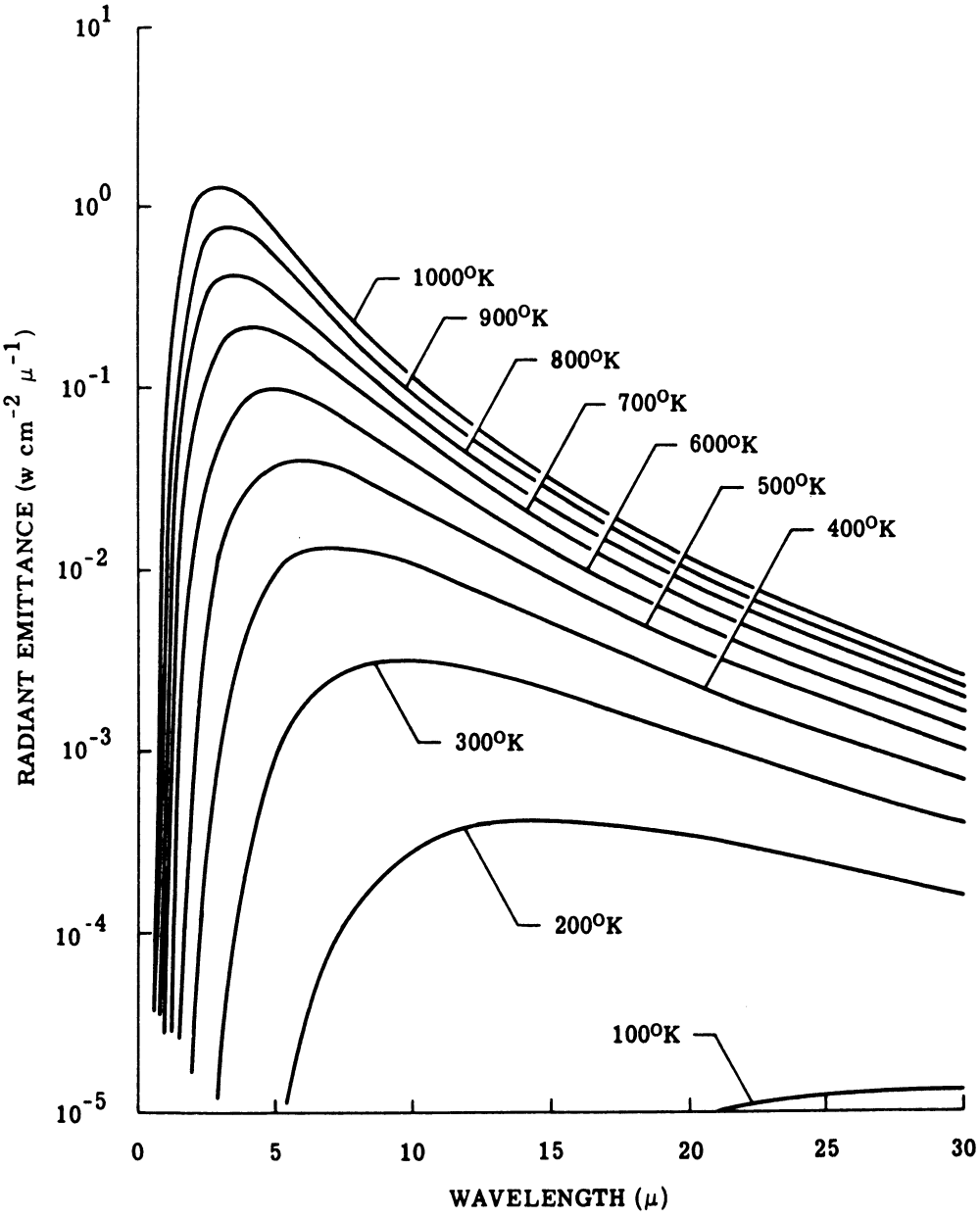

FIGURE 5. BLACKBODY RADIATION CURVES FOR 100°K TO 1000°K

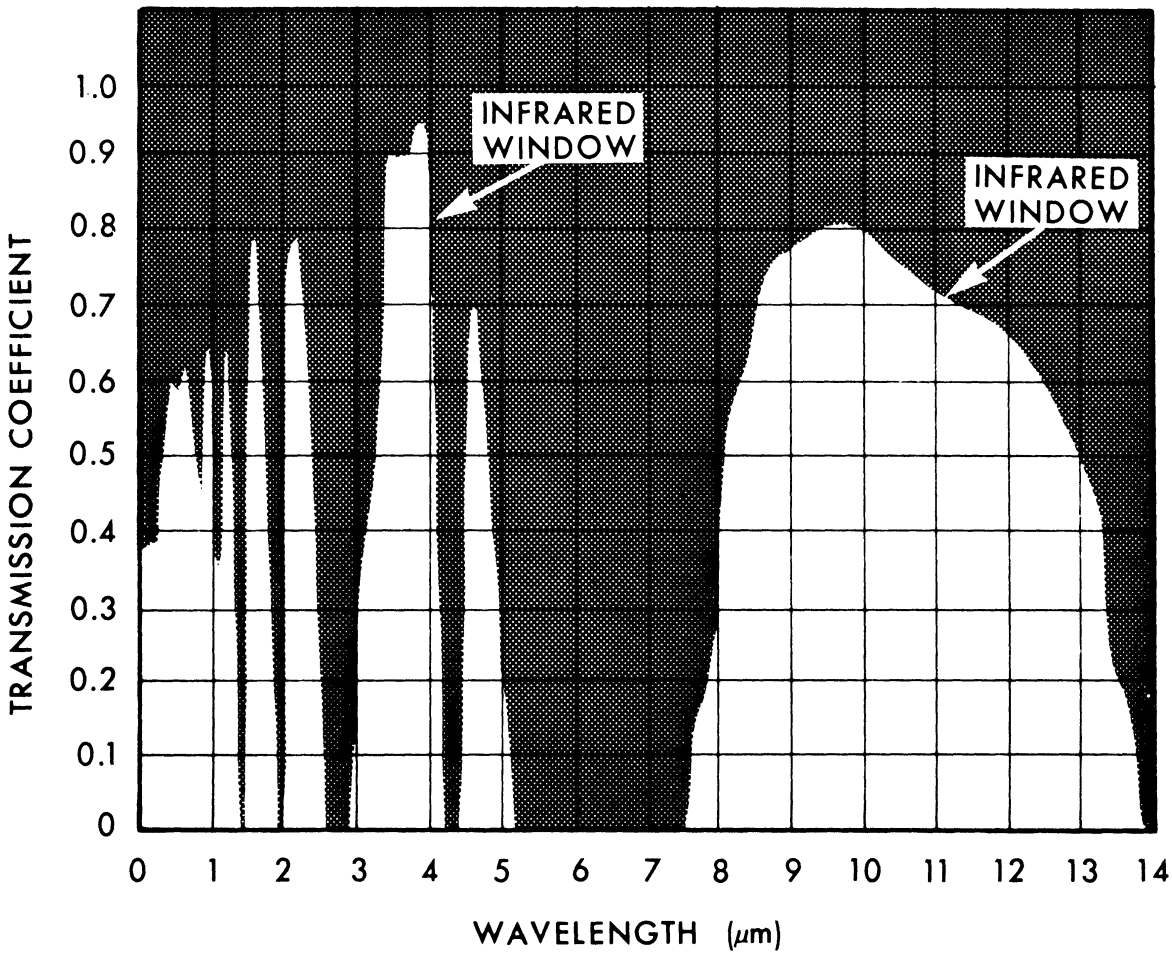

FIGURE 6. ATMOSPHERIC TRANSMISSION

As indicated above, the observed radiation of any real object (grey-body) is dependent in part on object emissivity. In the case of water, the emissivity in the 8-13.5 μm infrared range is very high. At 10 μm, the emissivity of pure water is 0.993, and at any particular wavelength in the 8-13.5 μm range, the emissivity ranges between 0.959 and 0.993. As a consequence of the high emissivity, it is frequently assumed that water may be treated as a blackbody. Although this assumption may at times be justified, accurate determinations of water temperature require that the "nonblackness" of water be considered in the analysis of data.

As a consequence of the various physical factors cited above, i.e., emissivity, atmospheric transmission, and wavelength peak, airborne infrared techniques for water temperature determination normally use a band or bands in the 8-13.5 μm spectral region. A 9.3-11.7 μm infrared channel was used in the thermal work described in this report.

As a general case, the radiation received by the detector will be modified to a small degree by the humidity of the intervening atmosphere, sky radiation, and other environmental factors. Corrections are applied to the radiometric temperatures as required.

4.2 PHYTOPLANKTON-CHLOROPHYLL

The relationship of the chlorophylls to phytoplankton production, phytoplankton activity, photosynthetic oxygen production, and state of eutrophication has been examined and reported by numerous investigators over the years [9, 10, 11]. Chlorophyll is widely used as an index of primary productivity of the photic zone and is a major parameter used in characterizing water masses.

The substances responsible for the absorption of light are the chlorophyll pigments, carotenoids, and special accessory pigments. Chlorophyll a is found in all green plants and is the predominant pigment in planktonic algae. Chlorophyll b appears to be present only in the Chlorophyceae, whereas chlorophyll c is found in several algae including all of the diatoms [12, 13]. Other major pigments are fucoxanthin found in the diatoms, phycoerythrin found in red algae, and phycocyanin found in red and blue-green algae. Spectral information of relevance to the problem under consideration is presented in Table 1 and illustrated, in part, in Figure 7. It should be noted in Figure 7 that major characteristics common to all species are found in the blue and red regions of the spectrum.

4.2.1 REFLECTANCE CHARACTERISTICS OF WATER CONTAINING PHYTOPLANKTON AND SUSPENDED SOLIDS

Both pure and polluted waters will absorb and scatter light. In the general case, scattering and absorption is caused by water molecules and by any suspended particulate materials present. The relative importance of scattering and absorption as mechanisms of attenuation is wavelength dependent, as shown in Figure 8.

The introduction of particulates (non-chlorophyll) into a body of water will result in the alteration of the reflectance spectra of the receiving waters in the manner shown in Figure 9. The illustration represents the case in which the receiving waters are clear, free of other pollutants, and of sufficient depth so that bottom reflectance is not a factor. Admittedly, the curves represent a somewhat simple and "ideal" case. However, the major point to be drawn from the curves

TABLE 1. SPECTRAL CHARACTERISTICS OF PIGMENTS

IN VIVO

WAVELENGTH (PEAK ABSORPTION)	PIGMENT
6750 - 6950 Å	CHLOROPHYLL *a*
ca. 4400 Å	
ca. 6500 Å	CHLOROPHYLL *b*
ca. 4650 Å	
ca. 6400 Å	CHLOROPHYLL *c*
ca. 5650 Å	
ca. 4700 Å	FUCOXANTHIN
ca. 5650 Å	PHYCOERYTHRIN
ca. 6200 Å	PHYCOCYANIN

SOURCE: STRICKLAND [12]
SELIGER AND MCELROY [13]

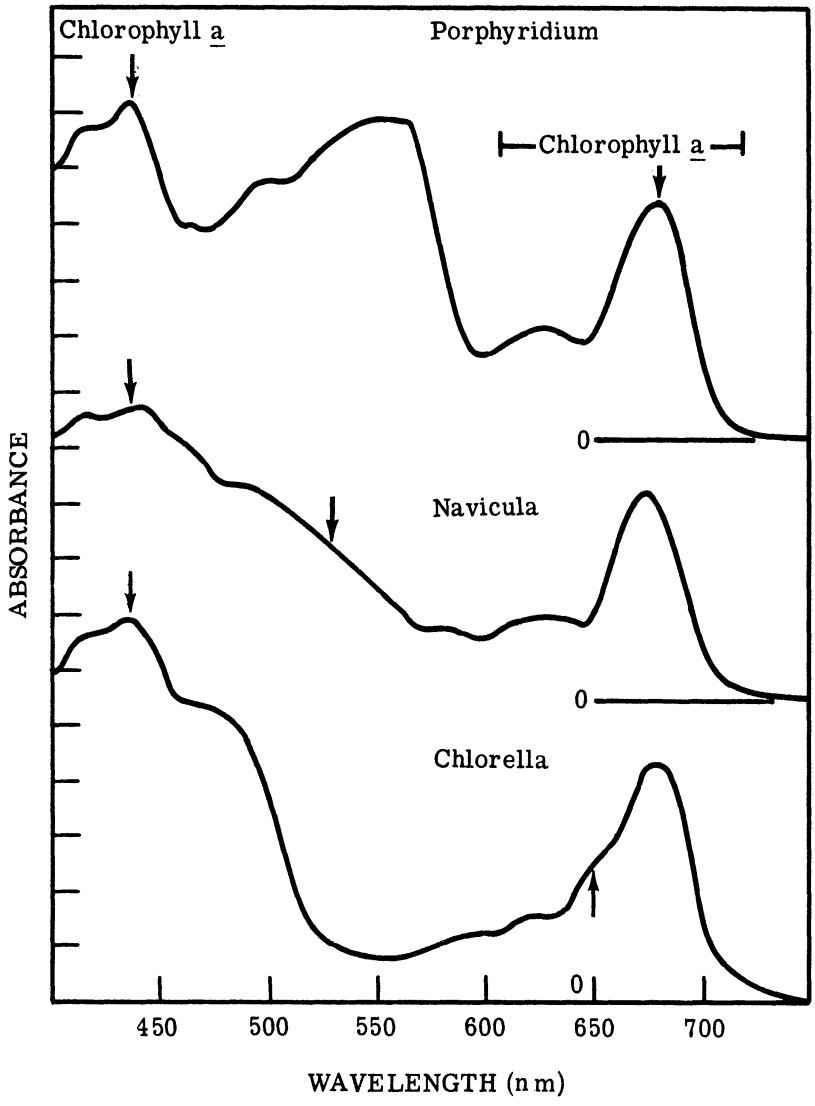

FIGURE 7. SPECTRA OF CHLORELLA VULGARIS, NAVICULA MINIMA AND PORPHYRIDIUM CRUENTUM. (Seliger and McElroy [13].)

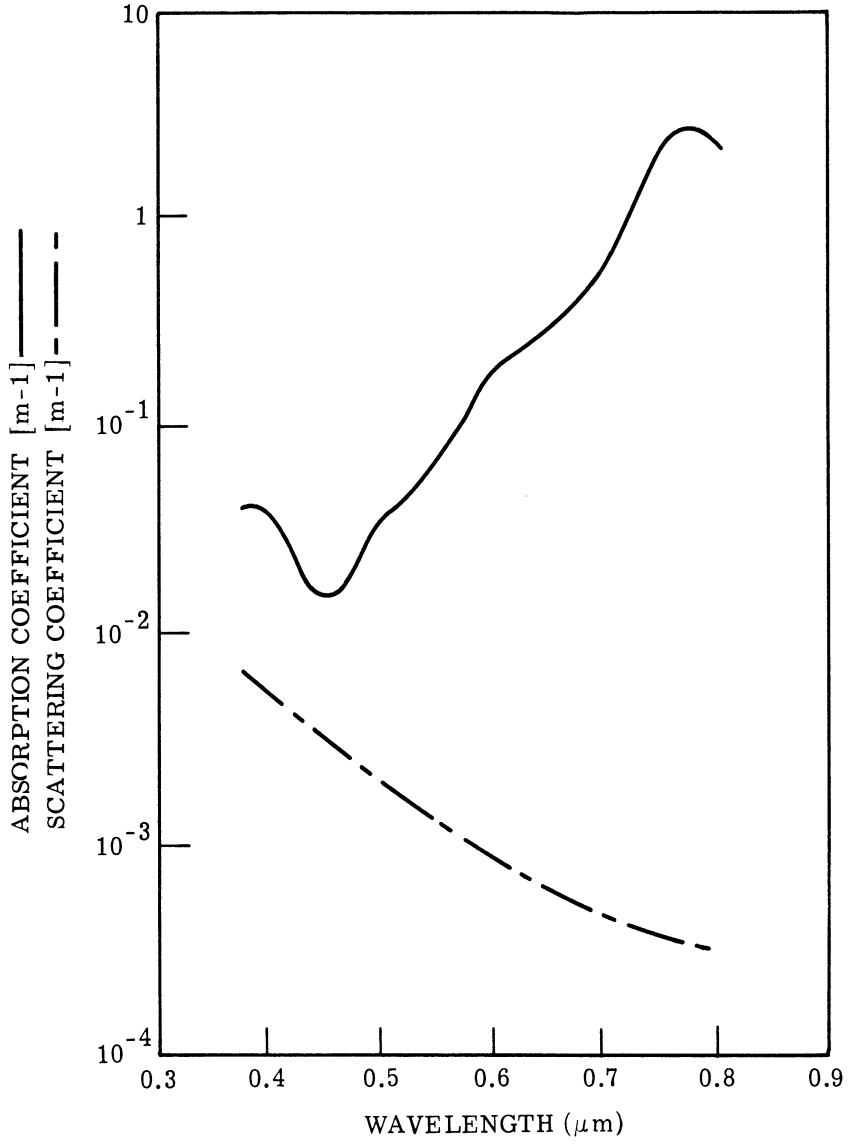

FIGURE 8. ABSORPTION AND SCATTERING COEFFICIENTS OF PURE WATER AS A FUNCTION OF WAVELENGTH. (After Gazey [14].)

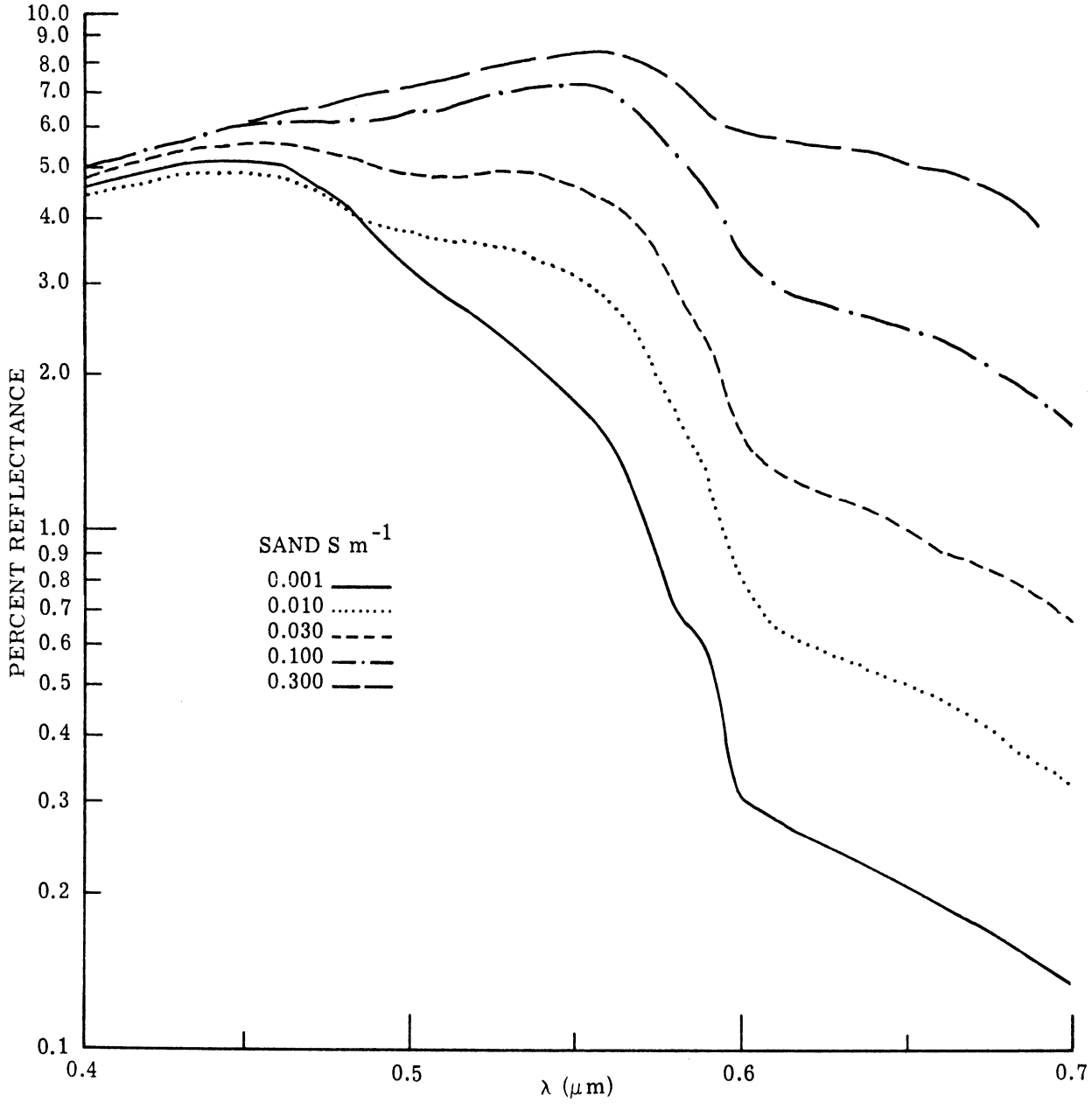

FIGURE 9. CALCULATED CHANGE IN REFLECTANCE OF OCEAN WATER WITH INCREASING CONCENTRATION OF SUSPENDED SOLIDS. (After G. Suits [15].)

is the fact that solids in suspension scatter light strongly (relative to pure water) particularly in the 0.6-0.7 μm spectral region. Secondly it should be noted that in the spectral region 0.4-0.5 μm, increases in the concentration of suspended solids (non-chlorophyll bearing) have little effect on the reflectance spectrum. Finally it should be stressed that the relationship shown is not linear and represents both particle size and concentration. Beyond 0.7 μm the curves for non-chlorophyll particulates drop off. Additionally the attenuation coefficient in the near-infrared will increase rapidly limiting observations to essentially the water surface.

Shown in Figure 10 is the expected spectral response for a body of water which contains varying concentrations of the more common phytoplankton. The nature of the response is due to the fact that phytoplankton are "particulates" and to the presence of photosynthetic pigments. The strong absorbance in the blue region of the spectrum is due largely to chlorophyll a and b. It should also be noted in Figure 10 that as the phytoplankton concentration increases towards bloom proportions, the reflectance increases in the red and near-infrared. The red/near-infrared relationship is opposite from the expected response for non-chlorophyll particulates. Although the attenuation coefficient is high in the near-IR, this region of the spectrum is potentially useful for the detection and analysis of phytoplankton blooms. No special significance is attached to the cross-over point at 0.51 μm in Figure 10. The location of the "hinge-point" and the position of the peak in the green band will vary with phytoplankton species and other characteristics of the water mass.

The foregoing remarks are presented simply to underscore the fact that in principle a basis exists for distinguishing between suspended

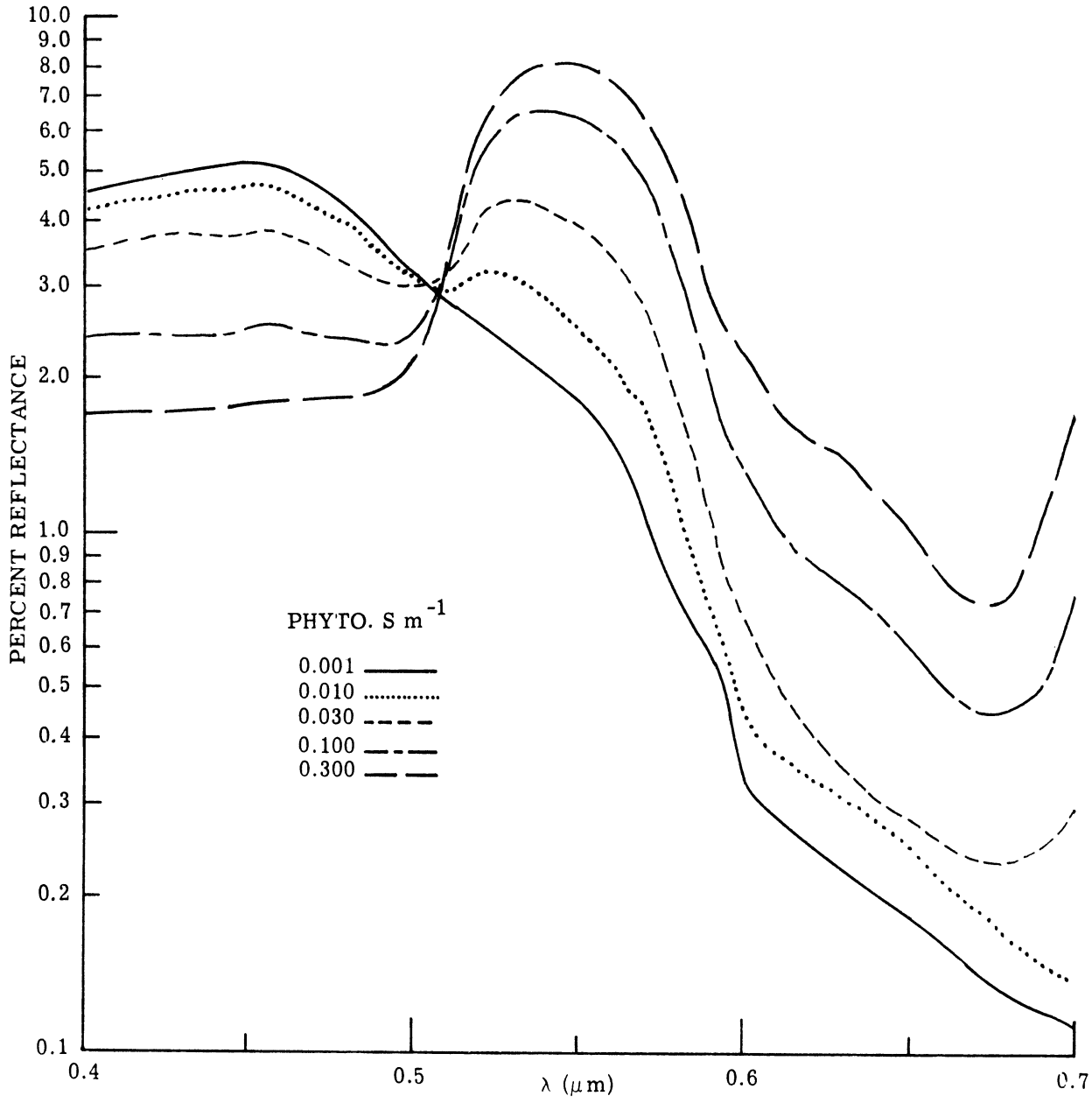

FIGURE 10. CALCULATED CHANGE IN REFLECTANCE OF OCEAN WATER WITH INCREASING CONCENTRATION OF PHYTOPLANKTON. (After G. Suits [15].)

solids and phytoplankton, through spectral analysis of remotely sensed data. In practice, however, the success achieved will be governed by the characteristics of the instrumental system, atmospheric conditions, selected spectral bands, and data processing procedures.

The basic relationships described above are illustrated in the figures which follow. In Figure 11 the relative change in reflectance due to suspended solids (sediments) is depicted in selected blue, green, and red spectral bands. As described earlier and illustrated in the calculated reflectance curves (Figure 9), the reflectance difference between high and low suspensions is minimal in the blue band and increases with increasing wavelength. Because of volume attenuation considerations, the practical upper limit to the above generalization is, at most, 0.7 μm.

Shown in Figure 12 is a section of shoreline of one of the Great Lakes in which the effects of chlorophyll (plankton) and suspended solids (sediments) on the reflectance of the water mass are clearly illustrated. Referring to the calculated reflectance curves (Figure 10), it should be noted that an increase in phytoplankton is accompanied by an increased reflectance in the red band and a decrease in the blue region of the spectrum. This is illustrated in Figure 12 along Section A-A. In the area dominated by suspended solids (Section B-B), the fundamental relationships between the blue and red bands for high and low (offshore) suspended solids concentrations is clearly evident.

As indicated earlier, reflectance in the near-infrared increases with increasing phytoplankton concentrations. Because of the high volume attenuation coefficient in the near-IR, measurements in this region are essentially restricted to bloom conditions.

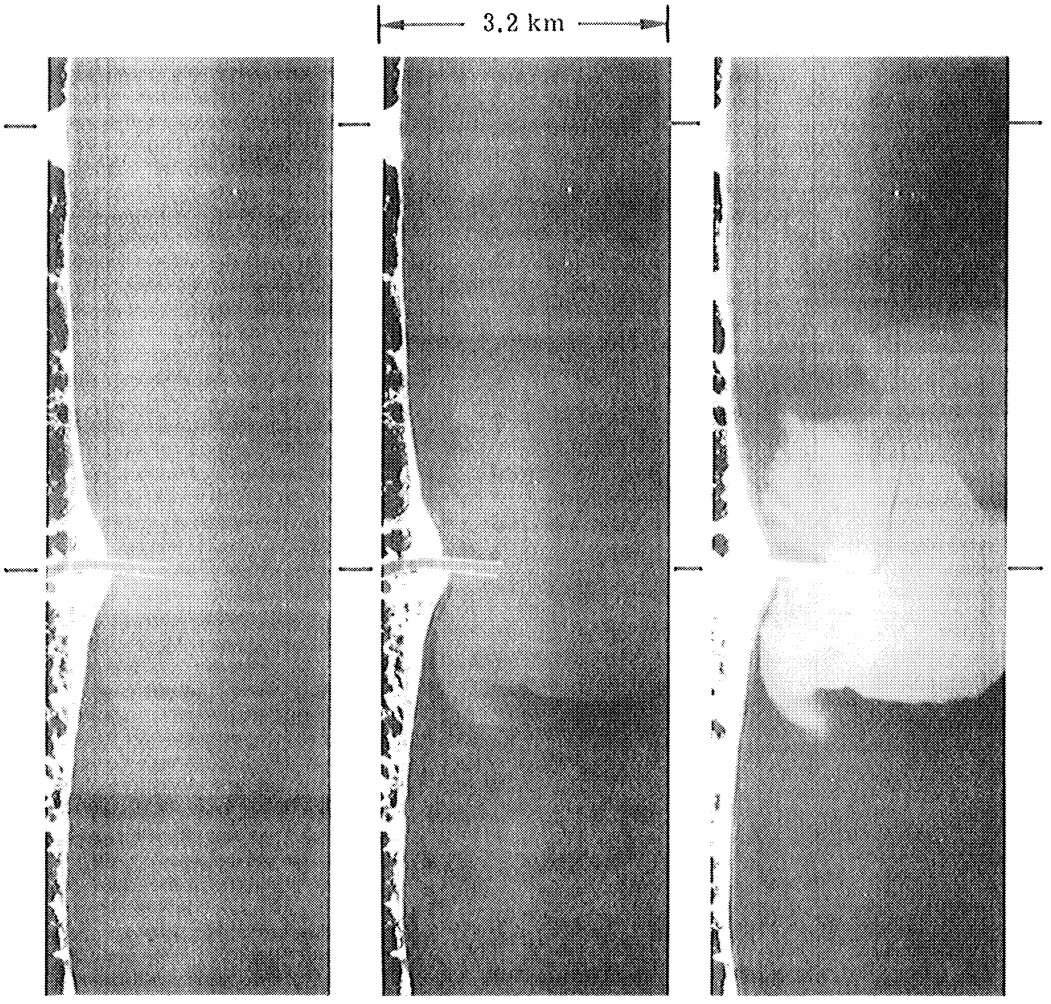

FIGURE 11. SUSPENDED SOLIDS.

Altitude = 1524 meters.

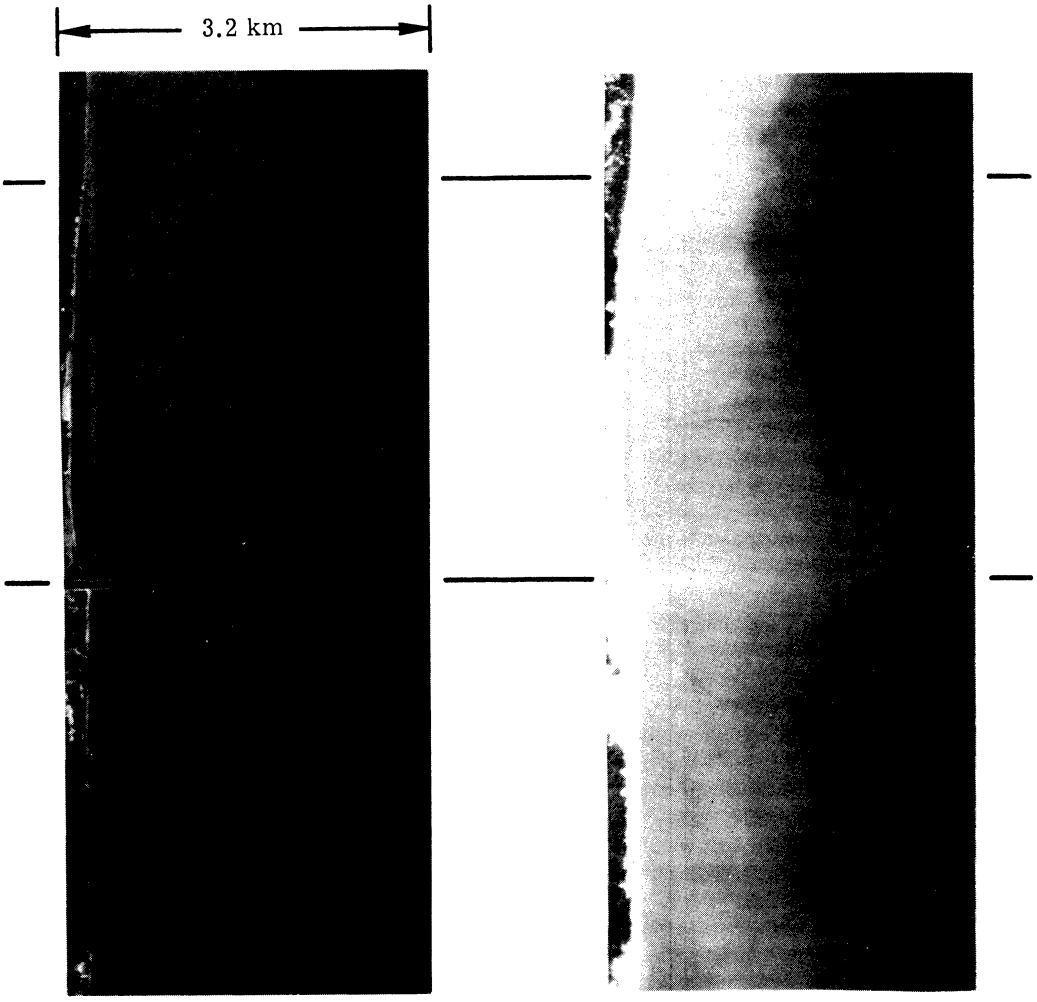

FIGURE 12. CHLOROPHYLL AND SUSPENDED SOLIDS.

Altitude = 1524 meters.

4.2.2 SPECTRAL ANALYSIS

From a remote sensing standpoint, two instrumental approaches are presently being investigated and/or utilized for *in vivo* chlorophyll measurement; (1) analysis of backscattered light and (2) measurement of fluorescence. To date, however, the major emphasis has been directed towards the use of passive techniques and the spectral analysis of backscattered light from the water body under investigation.

Clarke et al. [16] showed good correlation between shipboard measurement of chlorophyll and the spectra of backscattered light as measured from aircraft altitudes. Examining the spectral ratios 540 nm/460 nm, the authors found a decrease in reflectance at 460 nm and an increase in reflectance at 540 nm with increasing chlorophyll concentrations.

Work by Arvensen et al. [17] serves to further document use of the above ratioing technique. Using a differential radiometer operating at 443 nm and 525 nm, the authors were successful in measuring chlorophyll concentrations in the range 0.03 mg/m^3 - 10 mg/m^3. The authors report that more than 50 comparisons were made between remote measurements of chlorophyll from aircraft and laboratory analyses of samples. The results indicated an exponential relationship between the radiometer output signal and chlorophyll *a* concentration.

The developments reported by Clarke, et al. and Arvensen, cited above, represent important contributions to the remote sensing literature. However, the limitations of using spectral bands centered at 540 nm or 525 nm must be recognized. Due to water quality and phytoplankton species differences, the "hinge point" and the general reflectance curve in the green band will vary considerably.

Several other approaches to chlorophyll measurement must be cited. Savastano, et al. [18] used several algorithms including the following:

$$C = \alpha_1(R_{620} - R_{470})/R_{520} + \alpha_2$$

where R = radiance at 620 nm, 470 nm and 520 nm

α_1, α_2 = constants

The use of the radiance at 520 nm to normalize the data, assumes a hinge point at this wavelength. Mueller [19] used the principal components of the ocean color spectrum to develop empirical equations for chlorophyll and Secchi disc transparency. Mueller's technique was used for the analysis of oceanic waters at observed chlorophyll concentrations below 8.5 mg/m^3.

Wezernak [20] applied a technique in the study of a group of mesotrophic and eutrophic lakes which exploits the reflectance changes which occur in the red and blue regions of the spectrum. The basis for this approach is evident from an examination of Figure 10. With increasing phytoplankton concentrations, an increase in reflectance in the red band is accompanied by a decrease in the blue. The sharp rise in reflectance near 0.7 μm is another important feature which could be used in a chlorophyll model applied to eutrophic conditions. Because of path radiance considerations the use of a blue band is best suited for low altitude aircraft operations. The presence of "yellow substance" in significant amount will increase the absorbance in the blue region of the spectrum, however, the concurrent increase in the red band will not occur.

Shown in Figure 13 are two analog processed ratio images. The spectral bands used illustrate major qualitative differences in terms of transparency and chlorophyll. The main advantage of this type of processing is that

(a) Secchi Disk Transparency

$$\frac{\rho(0.50\ \mu m - 0.54\ \mu m)\ band}{\rho(0.62\ \mu m - 0.70\ \mu m)\ band}$$

(b) Chlorophyll a

$$\frac{\rho(0.62\ \mu m - 0.70\ \mu m)\ band}{\rho(0.42\ \mu m - 0.48\ \mu m)\ band}$$

FIGURE 13. ANALOG PROCESSED RATIO IMAGERY, TRANSPARENCY-CHLOROPHYLL

results are presented in the form of a photographic-type image. However, in order to display subtle differences and to provide quantitative results digital processing techniques are normally applied. The expression used in data processing to determine the surface chlorophyll distribution took the form:

$$\log CH_{RS} = a + b\ R_1$$

where CH_{RS} = chlorophyll *a*

a,b = constants

$$R_1 = \frac{\rho(0.62\ \mu m - 0.70\ \mu m)\ band}{\rho(0.42\ \mu m - 0.48\ \mu m)\ band}$$

The use of the above approach is intended primarily for use in relatively turbid or highly productive waters. As seen in Figure 14, the use of the red/blue spectral bands cited above, provides for nearly equal volume attenuation coefficients and restricts the remotely-sensed measurement to the near-surface. As a consequence, good correlations between surface chlorophyll and remote sensing data are normally obtained. Surface chlorophyll is defined in this case as chlorophyll found at approximately 1 meter in waters with high volume attenuation coefficients.

The use of the red/blue spectral pair may also be useful for chlorophyll analysis in relatively clear waters. The major constraint in using a red band, in this case, is the low reflectance normally found. Data presented by Duntley and co-workers [21] show the expected decrease in blue reflectance and an increase red reflectance with increasing surface chlorophyll concentration. Chlorophyll *a* concentrations (Figure 15) in the upper 6 to 8 meters were approximately 1.1 mg/m^3 at Station 5 and 1.8 mg/m^3 at Station 6C. This pattern in consistent with laboratory results [21]; whereas

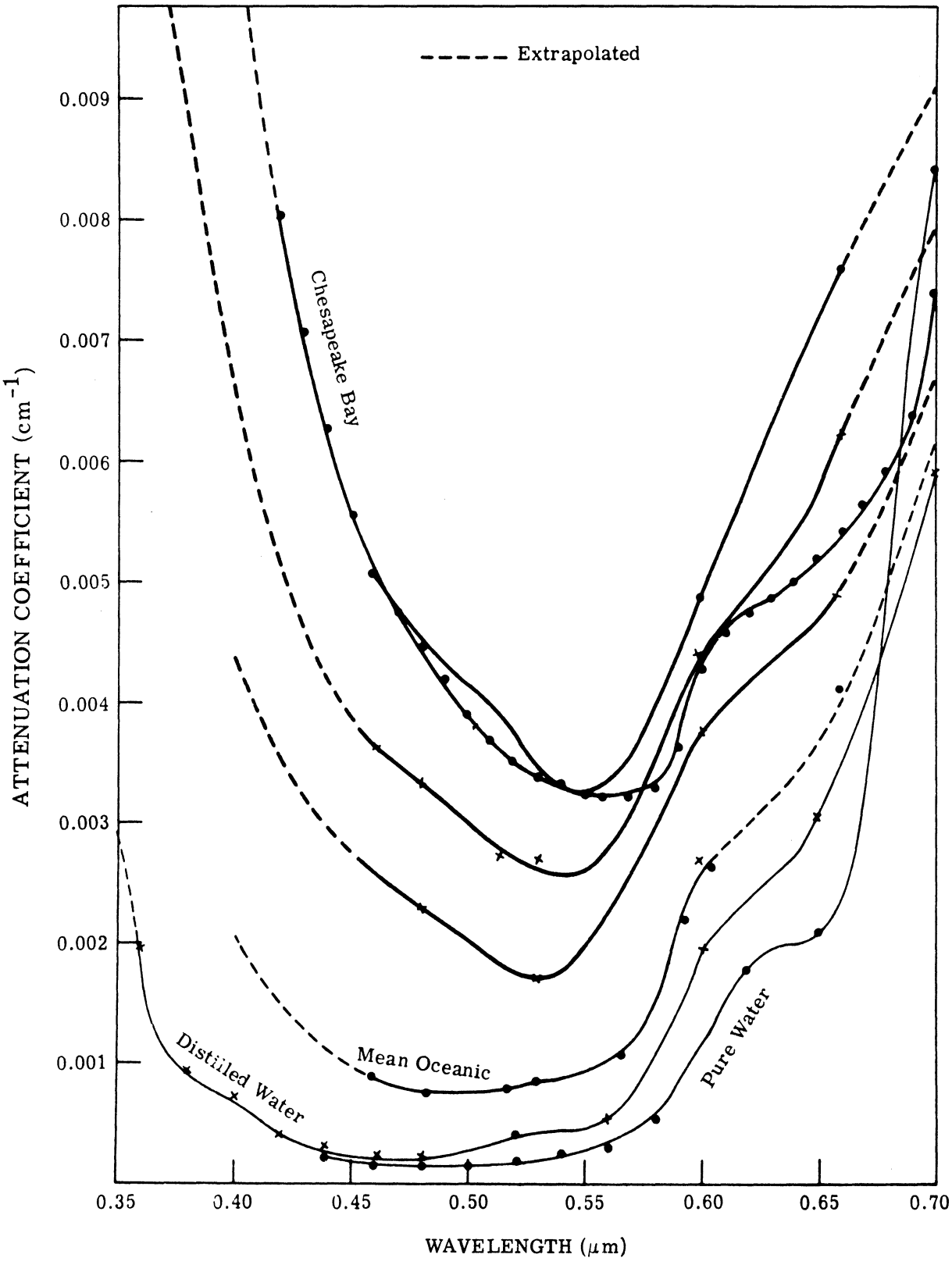

FIGURE 14. ATTENUATION-WAVELENGTH RELATIONSHIPS IN WATER

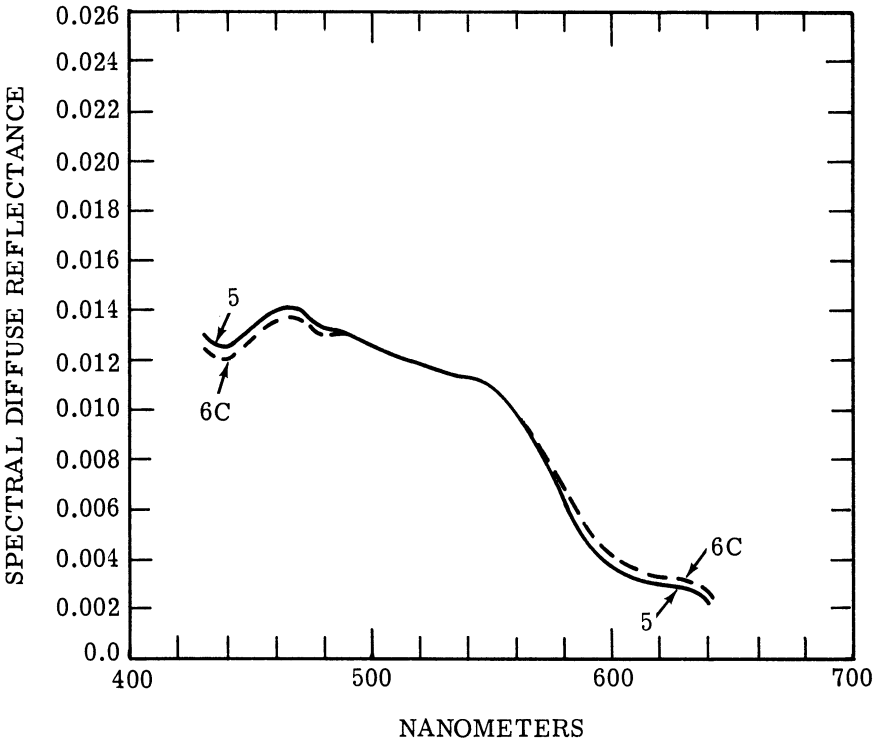

FIGURE 15. SUBSURFACE SPECTRAL DIFFUSE REFLECTANCE, TWO CHLOROPHYLL CONCENTRATIONS. (Source: Duntley, et al. [21].)

the comparisons made by Duntley and co-workers of the total integrated chlorophyll with spectral response, over a depth of 70 meters, provide contradictory results.

The fact that phytoplankton distribution is frequently very non-uniform in both the horizontal and vertical directions is well known and well documented in the literature [22]. This fact can make the analysis and interpretation of remote sensing data in clear waters extremely difficult. Since the signal recorded is related in an exponential manner to the distribution in a water column of less than Secchi disc depth, the integrating depth will in turn be related to the volume attenuation coefficient and spectral bands used. Phytoplankton stratification is most pronounced in oligotrophic waters. As a body of water increases in terms of phytoplankton productivity, the near-surface waters tend to exhibit less variance in terms of vertical distribution. Use of the blue-red band combination cited above, in a mesotrophic or eutrophic case tends to restrict the remotely sensed measurement to the near-surface. From an operational remote sensing standpoint, the use of spectral bands which restrict the measurement to the near-surface appears desirable.

The foregoing discussion serves to underscore the fact that no simple straightforward solutions to this extremely complex problem are possible. The "typical" curves shown in Figure 10 are representative, only in a very general sense, of water bodies containing the blue-green or green algae. No special significance should be attached to the cross-over point at 0.51 μm. Experience has shown that the shape of the curve and the position of the peak in the green region will vary due to various water quality factors and phytoplankton species differences. For example the presence of "red tide" in ocean waters will produce an important reflectance peak in

the 0.57-0.60 μm range. Hence for various taxonomic and water quality reasons, multispectral data collection is generally required and the use of narrow spectral bands (10 nm) is highly desirable. The use of instrumentation which offers a high signal-to-noise ratio and narrow spectral resolution permits an alternate approach to the analysis of data. This approach involves the use of the second derivative of the reflectance spectra.

In general, the derivative of a spectrum as a function of wavelength can be used to detect and resolve weak spectral features, overlapping lines, and subtle spectral differences [23]. White [24] points out that the second derivative of airborne data can provide spectra which are in close agreement with in situ measurements. When applied to chlorophyll analysis, the second derivative with respect to wavelength provides altitude-independent data of the water column. This results from the fact that the second derivative of path radiance may be assumed to be a linear function of wavelength over the region of interest, thereby making the second derivative of path radiance zero. In practice the technique is applied to a portion of the spectrum which exhibits an important inflection point.

Denoting wavelength and reflectance by λ and R respectively, the first derivative of reflectance at a wavelength between λ_i and λ_j is expressed as:

$$\frac{dR}{d\lambda} = \frac{R_j - R_i}{\lambda_j - \lambda_i}$$

Taking a portion of a reflectance curve described by reflectances R_1, R_2, R_3, at wavelengths λ_1, λ_2, λ_3; the first derivative at λ_2 may be expressed (approximately) as:

$$\frac{dR}{d\lambda}(\lambda_2) = \frac{1}{2}\left\{\frac{R_2 - R_1}{\lambda_2 - \lambda_1} + \frac{R_3 - R_2}{\lambda_3 - \lambda_2}\right\}$$

Therefore, the second derivative at λ_2 is:

$$\frac{d^2R}{d\lambda^2}(\lambda_2) = \frac{2}{\lambda_3 - \lambda_1}\left\{\frac{R_3 - R_2}{\lambda_3 - \lambda_2} - \frac{R_2 - R_1}{\lambda_2 - \lambda_1}\right\}$$

The same result can be obtained by fitting the three points (λ_1, R_1), (λ_2, R_2) and (λ_3, R_3) to a parabola and determine the second derivative of the parabola at λ_2, as follows:

1. Parabola;

$$R(\lambda) = a + b\lambda + c\lambda^2$$

$$R_1(\lambda_1) = a + b\lambda_1 + c\lambda_1^2$$

$$R_2(\lambda_2) = a + b\lambda_2 + c\lambda_2^2$$

$$R_3(\lambda_3) = a + b\lambda_3 + c\lambda_3^2$$

Solving, $\frac{R_2 - R_1}{\lambda_2 - \lambda_1}$, $\frac{R_3 - R_2}{\lambda_2 - \lambda_1}$, and calculating c;

$$c = \frac{(R_3 - R_2)}{(\lambda_3-\lambda_2)(\lambda_3-\lambda_1)} - \frac{(R_2 - R_1)}{(\lambda_2-\lambda_1)(\lambda_3-\lambda_1)}$$

3. Since $\frac{d^2R}{d\lambda^2}(\lambda_2) = 2c$, $\frac{d^2R}{d\lambda_2} = \frac{2}{(\lambda_3 - \lambda_2)} \left\{ \frac{R_3 - R_2}{\lambda_3 - \lambda_2} - \frac{R_2 - R_1}{\lambda_2 - \lambda_1} \right\}$

From an operational remote sensing standpoint, implementation of the technique requires narrow spectral band and a high signal-to-noise ratio.

4.3 TRANSPARENCY

The term transparency as used in this report refers to Secchi disc transparency. As an optical parameter, Secchi disc transparency is a function of absorption and scattering by materials in solution and suspension; and generally related to the volume attenuation coefficient in the green spectral region.

As indicated earlier, Mueller [19] used principal component analysis of ocean color spectra to develop an empirical equation for Secchi disc transparency. Wezernak [20] utilized reflectance data in the green and red regions of the spectrum in transparency analysis. The expression used to calculate transparency was:

$$\log T_{RS} = c + dR_2$$

where T_{RS} = Secchi disc transparency

c,d = constants

$R_2 = \frac{(0.50\ \mu m - 0.54\ \mu m)\ band}{(0.62\ \mu m - 0.70\ \mu m)\ band}$

The green band used generally corresponds to the region of minimum attenuation in productive and moderately turbid waters (Figure 14). With increasing substances in suspension, the above ratio (and transparency) decrease.

5

RESULTS AND DISCUSSION

Reported in the section which follow are the results of the remote sensing program of data collection and analysis conducted by ERIM. The findings which follow are for 7 April 1973 and result from a multispectral aircraft mission at an altitude of 3048 meters, together with selected ERTS-1 data.

The investigations undertaken by ERIM represent one phase of the intensive field and remote sensing program conducted or supported by NOAA/NESS at this location.

5.1 OCEAN DUMPING ACTIVITIES

Waste fields created by barge dumping of acid-iron waste were clearly in evidence in the study area. Acid-iron waste in the process of being discharged, recently dumped waste, as well as relatively old waste suspensions have been detected.

As the acid-iron wastes are dumped into the marine environment a series of chemical reactions take place during which the acid is neutralized and the ferrous iron is rapidly oxidized to the ferric state, as shown in the following equations:

$$2FeSO_4 + 2H_2SO_4 + O_2 \rightarrow Fe_2(SO_4)_3 \downarrow + H_2O + H_2SO_4$$

$$Fe_2(SO_4)_3 + 6H_2O \rightarrow 2Fe(OH)_3 \downarrow + 3H_2SO_4$$

Shown in Figure 16 is a typical acid-iron dumping operation in progress. The waste solution changes in appearance from a green-yellow color to orange as the material undergoes oxidation from the ferrous to the ferric state. Due to the low solubility of iron at the pH of seawater, precipitates are formed. The ferric compounds produced tend to remain in suspension for considerable periods of time. The oxidized waste field is yellow or orange in color. Shown in Figure 17 is a portion of a residual field at the time of the satellite pass over the study area (E-1258-15082).

The dye markers in Figure 16 depict a general southwesterly movement of the waste field during an outgoing tide at Sandy Hook. The tendency for the waste field to move in a southwesterly direction (towards shore) was also supported by field observations on 25 April 1973. The westerly edge of a large dispersed yellow water mass (acid-iron waste) was located on that date at a position approximately 10 km. off the New Jersey coast.

Field data were collected in support of the program at the locations shown in Figure 18. Typical surface water quality determinations for the study area are presented in Table 2. As expected, a sharp increase in total iron is found in the acid grounds area. Typical concentrations in old residual fields were found to be approximately 800 µg/ℓ. This compares with 20 µg/ℓ in adjacent ocean waters. Most of the iron is in the form of particulate iron.

The values identified as "sewage sludge" in Table 2 refer to the area designated for this purpose and do not represent values for the sludge itself. The sludge as it is being dumped is generally dark in color (digested sludge), high in total solids and includes digester supernatant. The settleable solids settle out rapidly leaving an increased concentration of suspended solids in the overlying waters and a variable amount of floatable substances in the area.

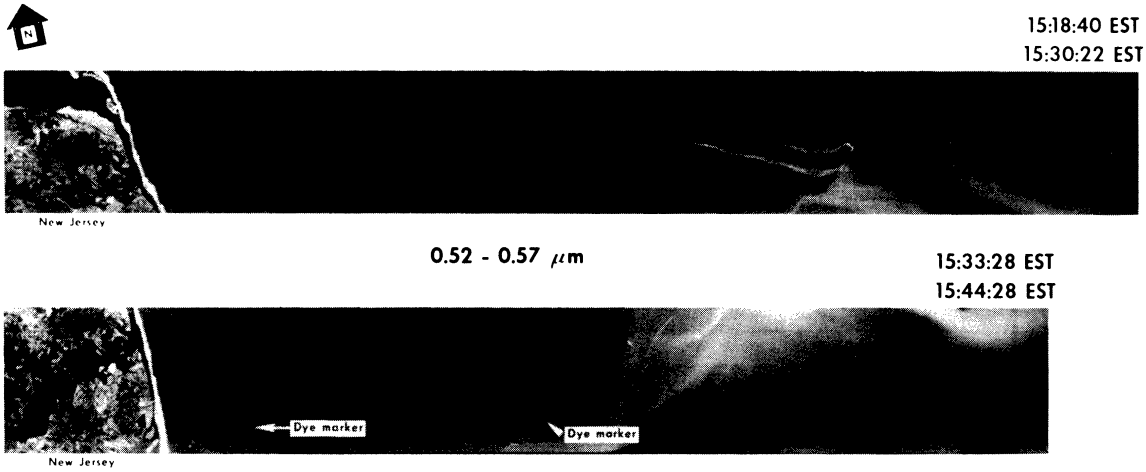

FIGURE 16. ACID-IRON WASTE, NEW YORK BIGHT, 7 APRIL 1973, P.M.
Aircraft imagery altitude = 3048 meters.

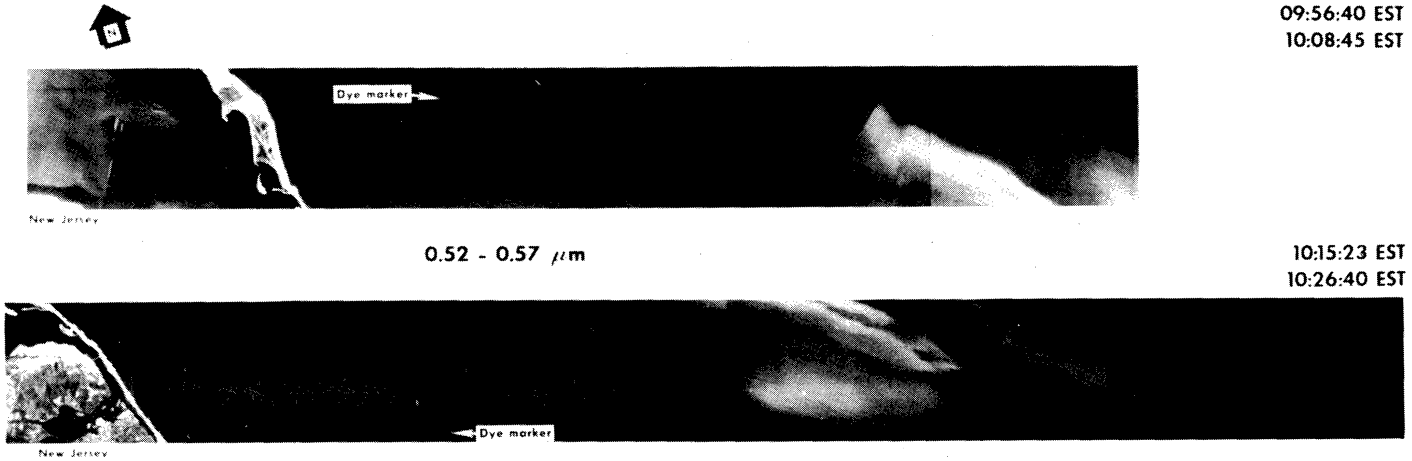

FIGURE 17. ACID-IRON WASTE, NEW YORK BIGHT, 7 APRIL 1973, A.M.
Aircraft imagery altitude = 3048 meters.

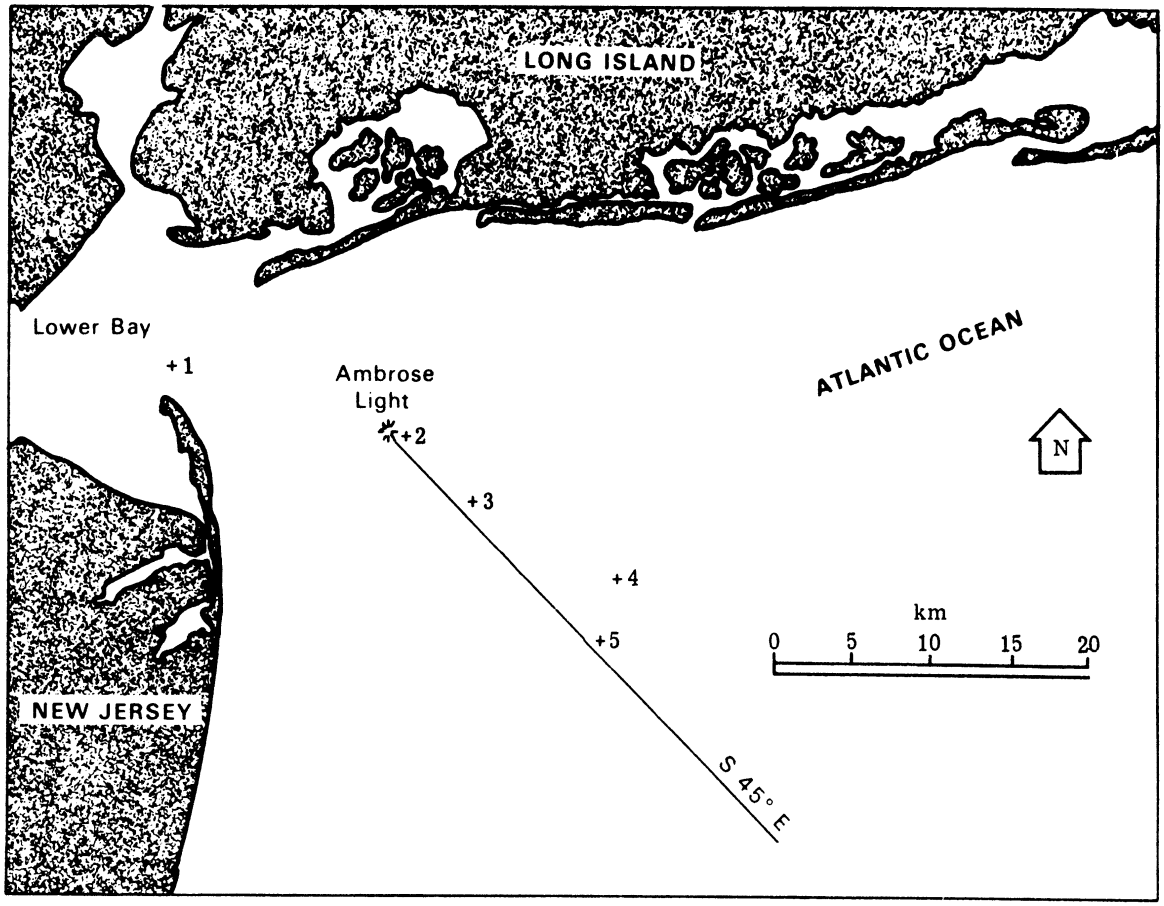

FIGURE 18. LOCATION OF SAMPLING STATIONS, NEW YORK BIGHT

TABLE 2. SURFACE WATER QUALITY DATA

STATION	pH	TURBIDITY JTU	SUSP. SOLIDS mg/ℓ	TOTAL SOLIDS gm/ℓ	SALINITY 0/00	CHLORO-PHYLL a mg/m^3	PO_4-P µg/ℓ	TOTAL Fe µg/ℓ	SECCHI DISK (METERS) WHITE	BLACK
1 (outgoing tide)	8.0	6.6	14	18.4	17	35	100	--	1.07	0.61
2 Ambrose Tower	8.1	3.7	7	26.0	24	4	20	--	3.05	1.52
3 Sewage Sludge Dump Area	8.0	7.0	31	31.7	28	1	140	--	1.07	0.46
4 Ocean Background	8.0	1.3	4	33.4	31	1.4	15	20	6.40	2.44
5 Residual Acid-Iron Field	8.0	2.9	6.5	33.7	30	0.9	5	800	2.44	1.52

5.2 MOVEMENT OF WATER MASSES AS EVIDENCED BY SEA SURFACE TEMPERATURE, DYE TRACER, AND TURBIDITY PATTERNS.

During the course of the remote sensing data collection program on 7 April 1973, high-water and low-water elevations at Sandy Hook occurred at 1044 EST and 1641 EST, respectively. Surface circulation patterns during an out-going tide and an incoming-tide are depicted in the imagery which follows.

The ability to measure small temperature differences can be utilized in the analysis of a number of oceanographic problems including analysis of circulation dynamics. Shown in Figure 19 is a thermal image (9.3-11.7 μm) of the study area during an outgoing tide. The highly complex surface circulation in the lower bay and adjacent areas is clearly depicted. The sharp thermal discontinuities provide information about flow direction, mixing, and water mass convergence. Surface temperature distribution is depicted in Figure 20.

Additional data regarding surface circulation is obtainable through an analysis of Figures 21 and 22. The dye implants indicate a general clockwise surface circulation in the Bight. Comparable data during the incoming portion of the tidal cycle is presented in Figures 23 through 26.

From a water quality or resource management standpoint, information regarding the movement of water masses is vital to any program designed to evaluate the chemical-biological status of the resource, to evaluate the effects of pollution loading, or to plan programs of corrective action. The remotely sensed information presented in Figures 19 through 26 underscores the necessity of integrating remotely sensed information with chemical and biological data collected by conventional shipboard techniques in environmental analyses. All too frequently data collected by conventional point sampling techniques in a highly dynamic estuarine environment results

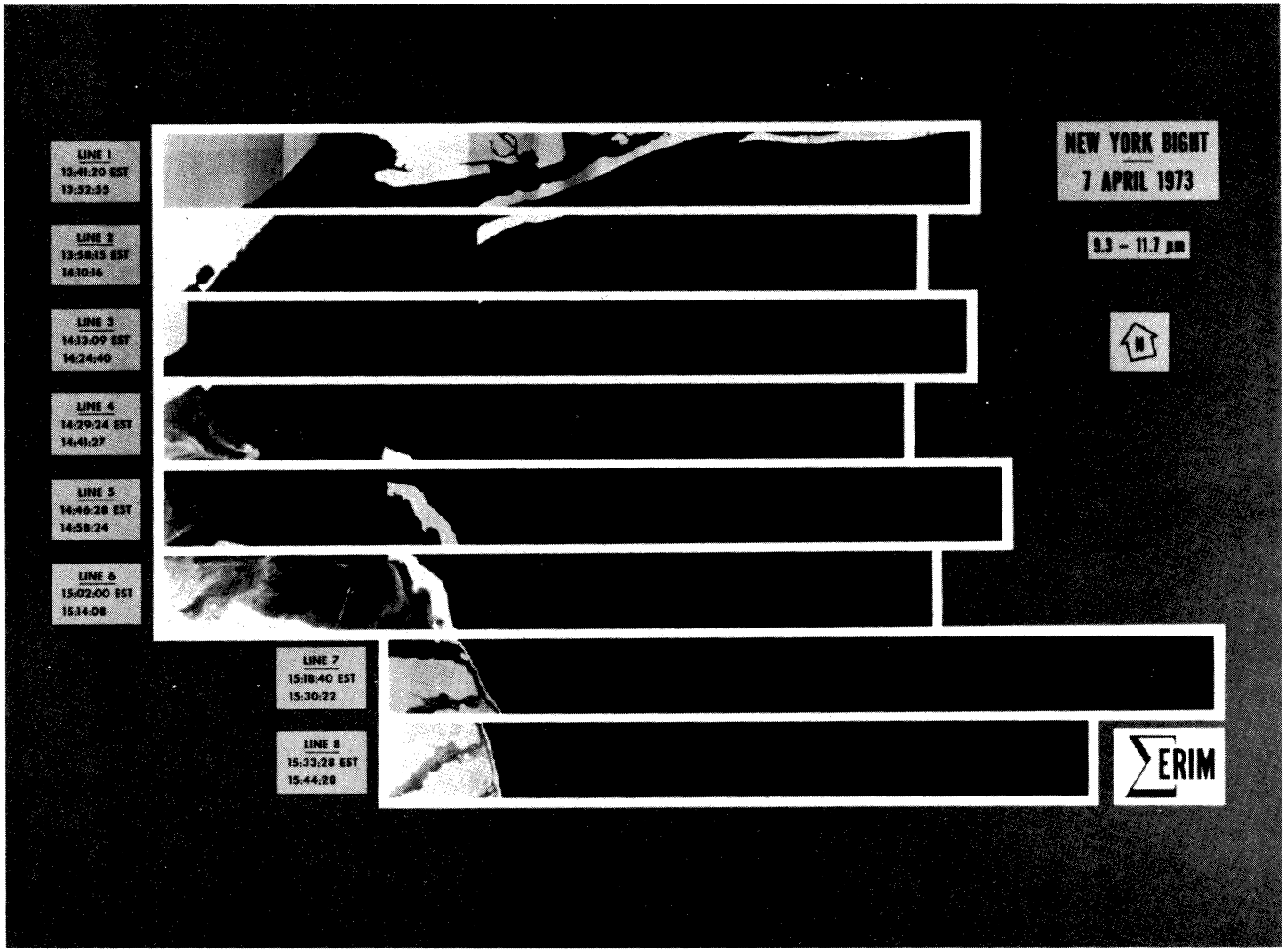

FIGURE 19. AFTERNOON DATA (9.3-11.7 μm)

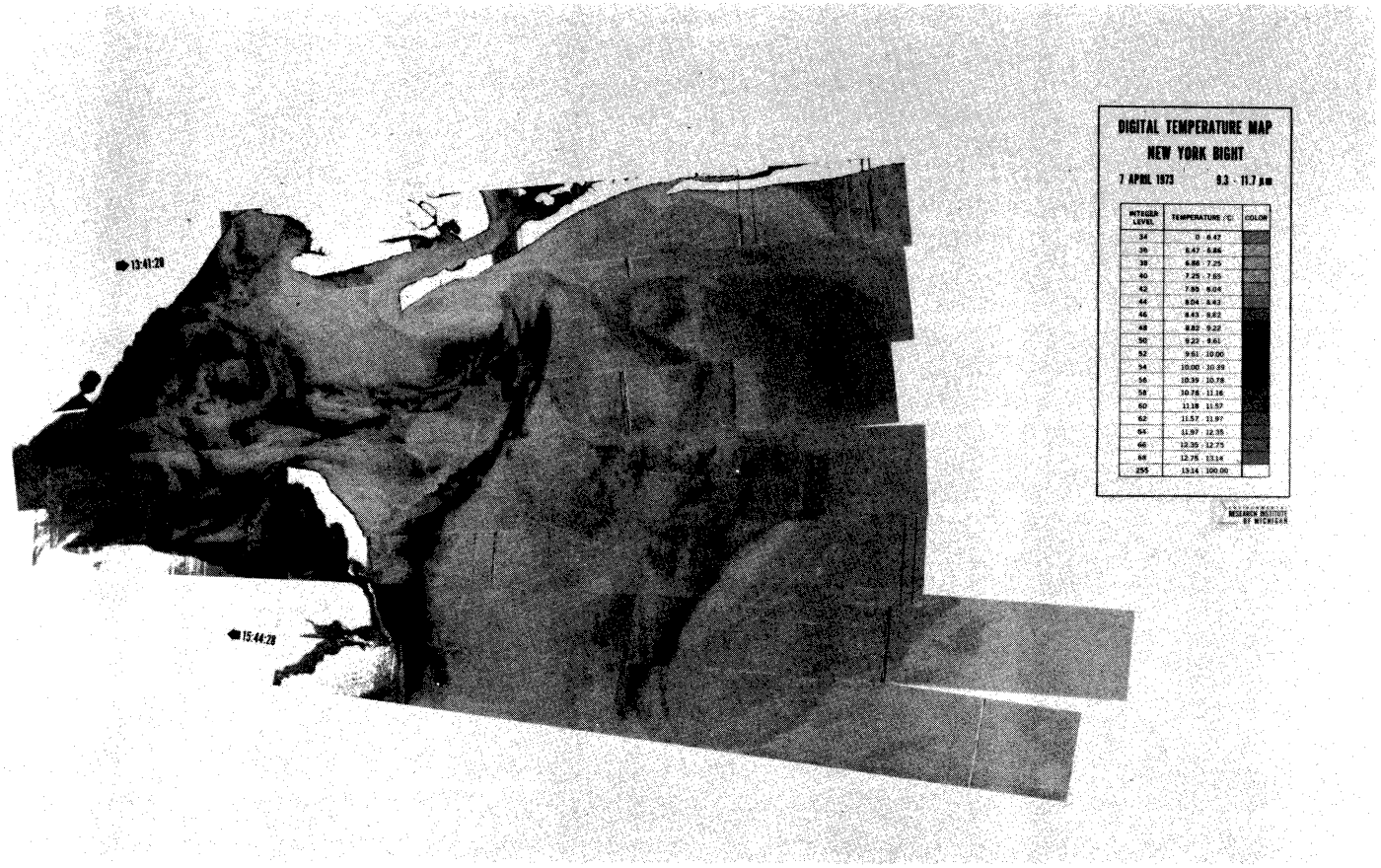

FIGURE 20. DIGITAL TEMPERATURE MAP - AFTERNOON DATA

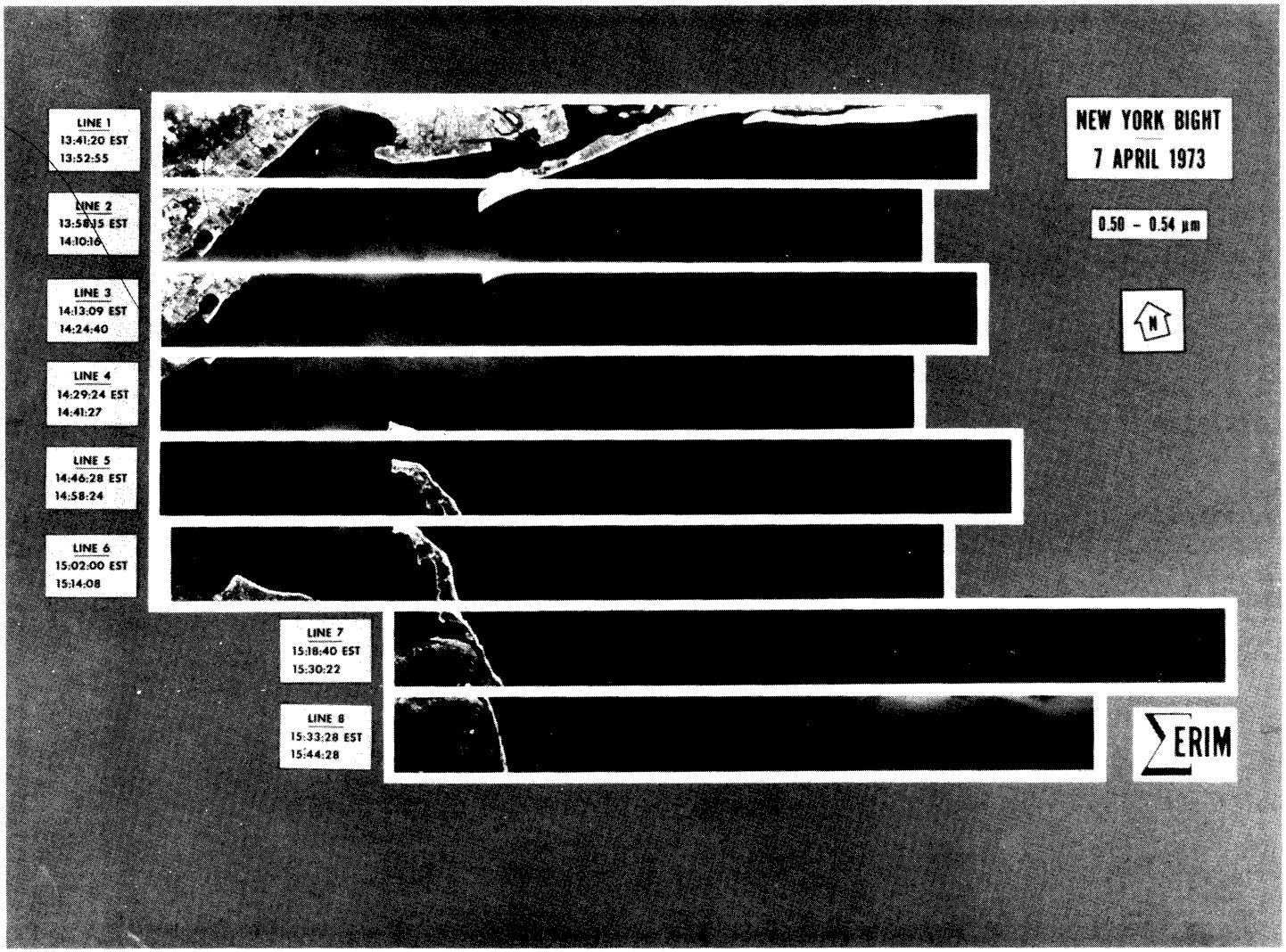

FIGURE 21. AFTERNOON DATA (0.50-0.54 μm)

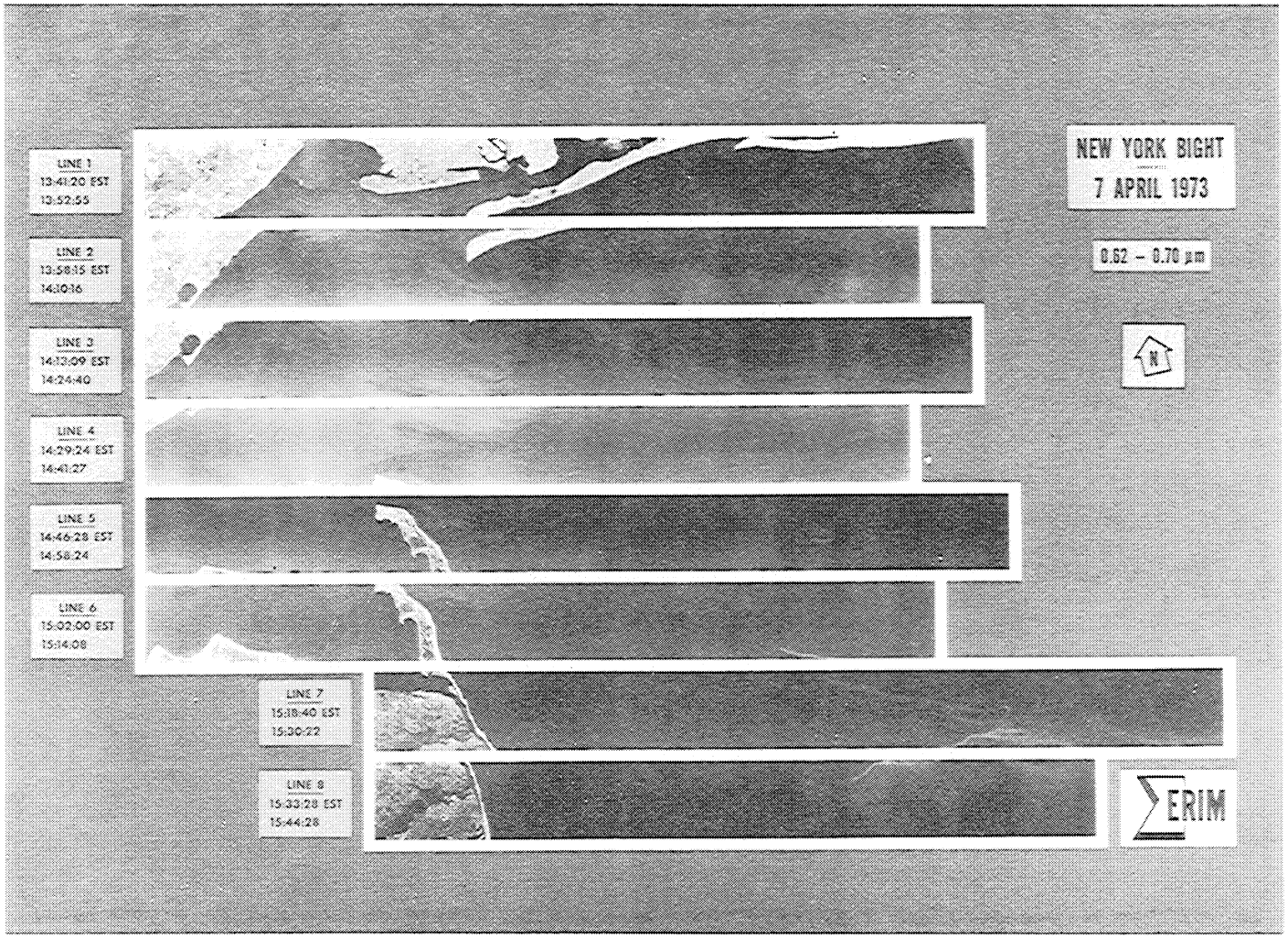

FIGURE 22. AFTERNOON DATA (0.62-0.70 μm)

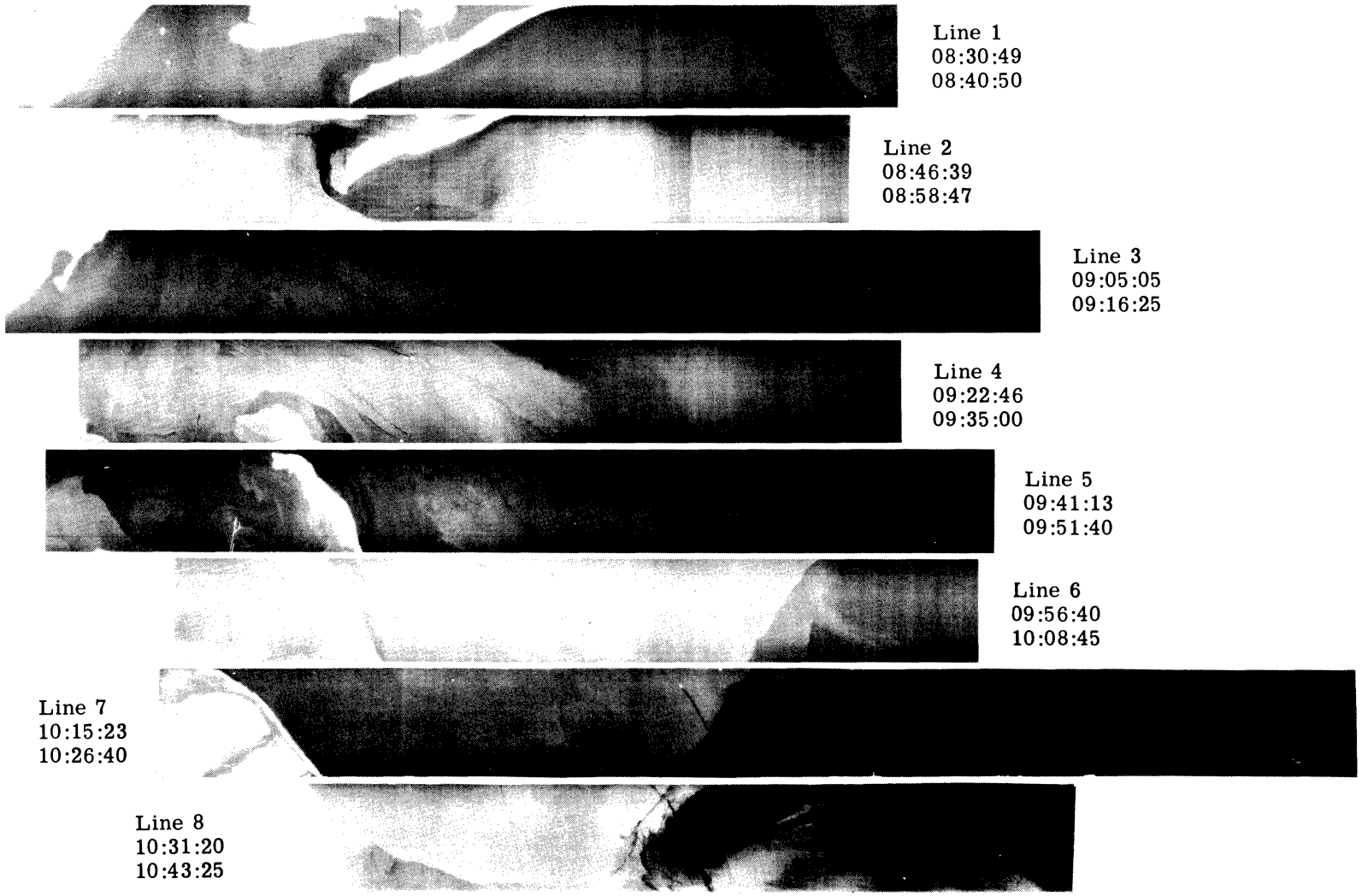

FIGURE 23. MORNING DATA (9.3-11.7 μm)

0.62-0.70 μ
7 April 1973

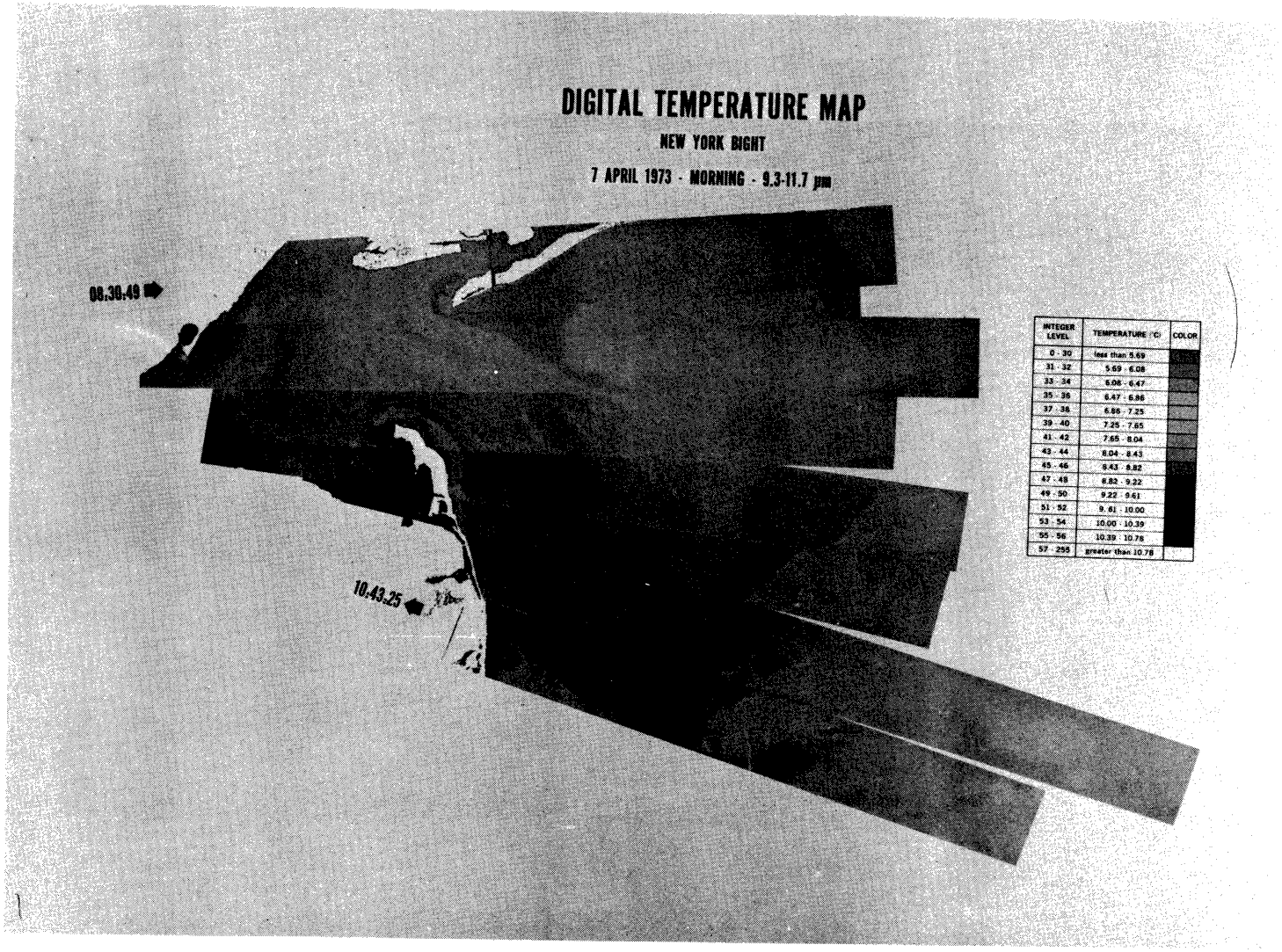

FIGURE 24. DIGITAL TEMPERATURE MAP - MORNING DATA

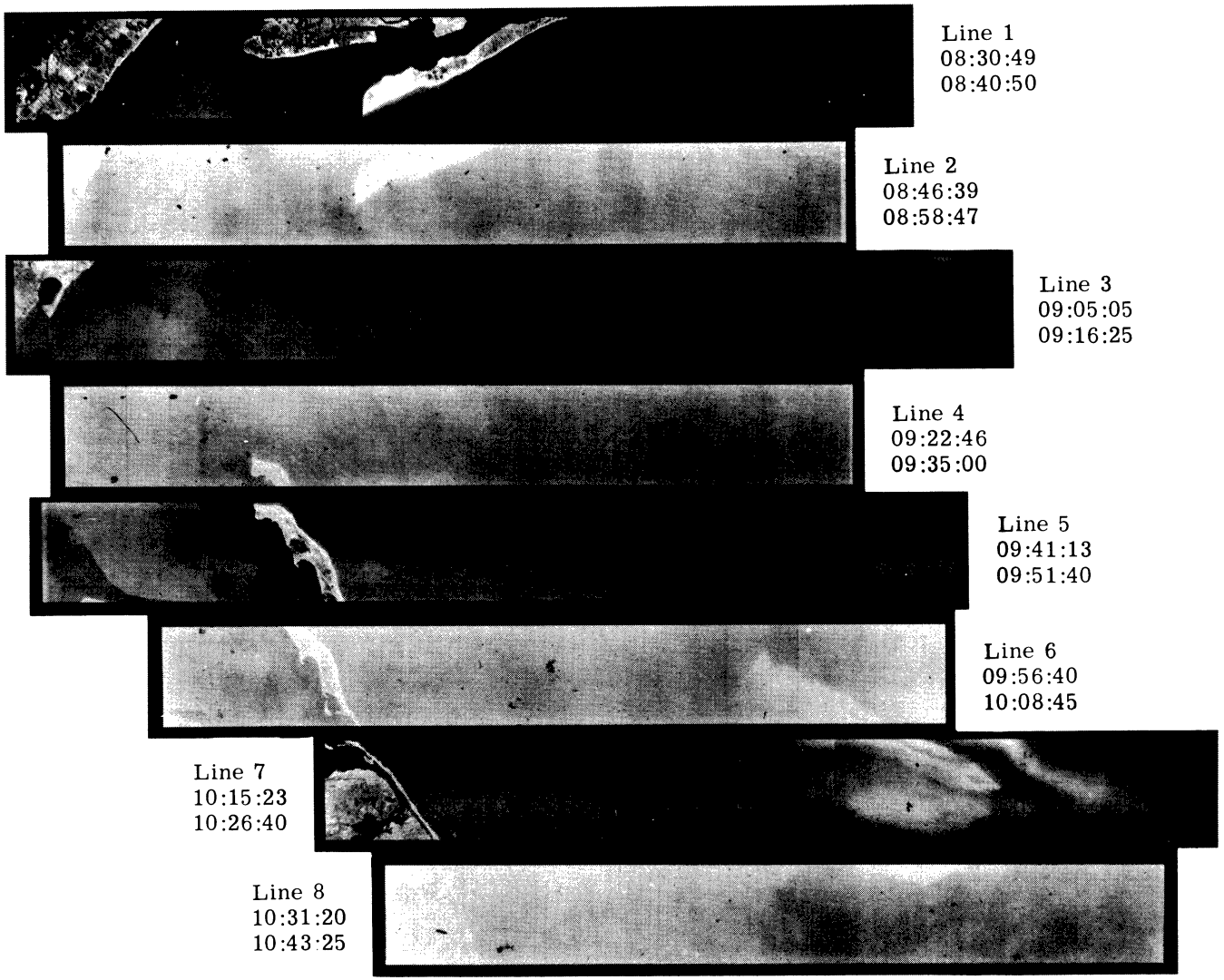

FIGURE 25. MORNING DATA
(0.52-0.57 μm)

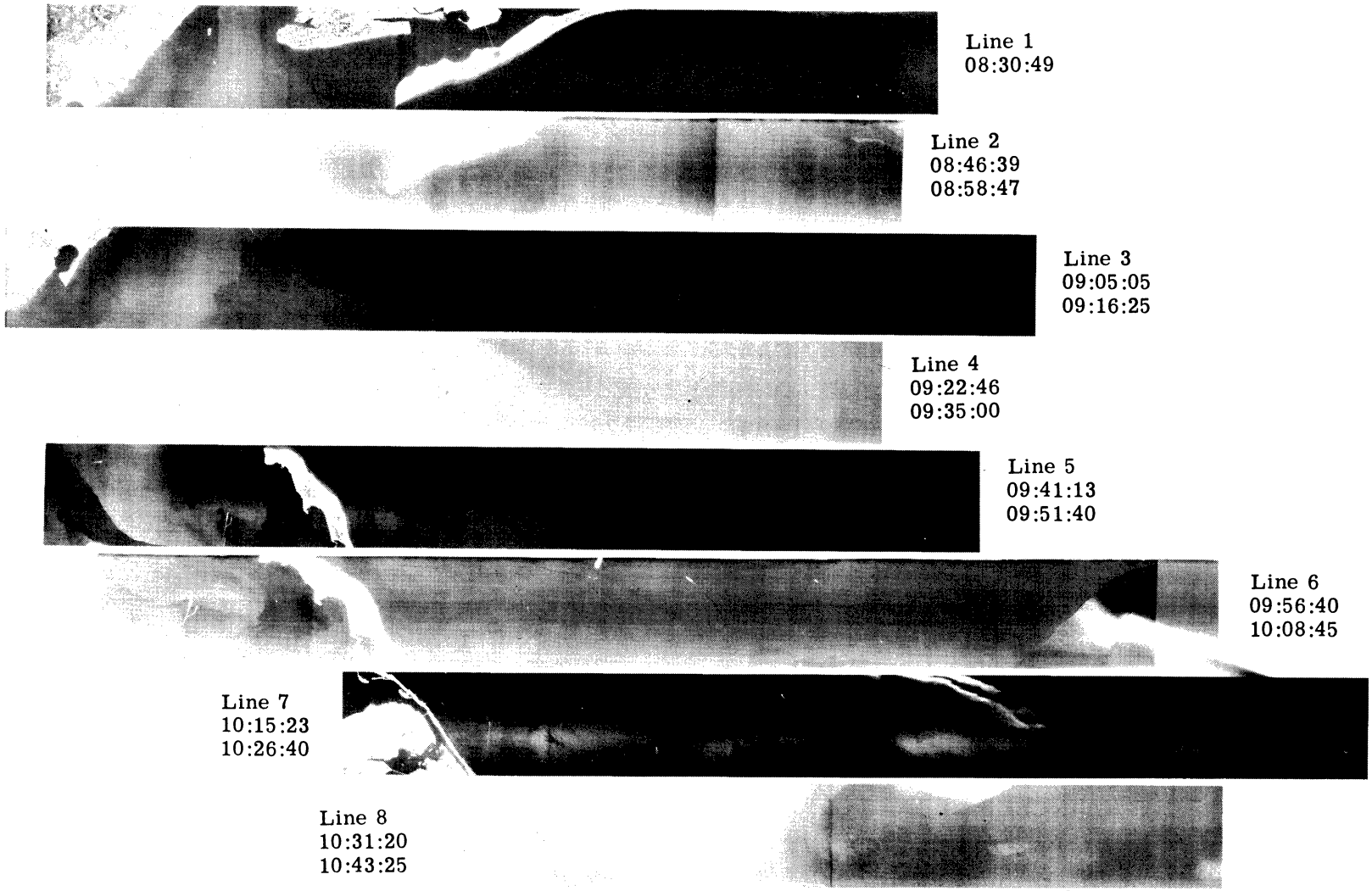

FIGURE 26. MORNING DATA (0.62-0.70 μm)

0.62 - 0.70 μ
7 April 1973

in a disjointed mosaic of data, which is difficult or impossible to interpret, and therefore, has little practical significance.

5.3 CHLOROPHYLL AND TRANSPARENCY

The problem of ocean color analysis is extremely complex due to the fact that the aquatic environment is a complex heterogeneous system in terms of its chemistry and biology. As a consequence no simple, straightforward, universal solutions to the problem of chlorophyll and transparency analysis are possible. All attempts to measure these parameters through remote sensing have involved empirical or semi-empirical methods.

The techniques adopted in this program are based on the considerations discussed in Section 4. The expressions used for determining surface chlorophyll _a_ and transparency were:

1. $CHA = 10^{a + b \bar{R}_1}$

   where

   CHA = chlorophyll _a_, mg/m^3

   a,b = constants

   $\bar{R}_1 = \frac{\rho(0.62\text{-}0.70\ \mu m)\ channel}{\rho(0.42\text{-}0.48\ \mu m)\ channel}$

2. $T = 10^{c + d \bar{R}_2}$

   where

   T = Secchi disc transparency

   c,d = constants

   $\bar{R}_2 = \frac{\rho(0.50\text{-}0.54\ \mu m)\ channel}{\rho(0.62\text{-}0.70\ \mu m)\ channel}$

The constants used in the above expression were determined from an analysis of an inland lake data set [20] and found to be applicable to other similar situations including the New York Bight. The expressions are intended for use in productive waters with Secchi disc transparencies of less than 6 meters. The expressions used in data processing were:

3. $CHA = 10^{5.5668\ \bar{R}_1 - 2.4761}$

where

CHA = chlorophyll a, mg/m^3

$\bar{R}_1 = \frac{\rho(0.62\text{-}0.70\ \mu m)\ channel}{\rho(0.42\text{-}0.48\ \mu m)\ channel}$

4. $T = 10^{0.8788\ \bar{R}_2 - 0.6235}$

where

T = Secchi disc transparency, ft.

$\bar{R}_2 = \frac{\rho(0.50\text{-}0.54\ \mu m)\ channel}{\rho(0.62\text{-}0.70\ \mu m)\ channel}$

The reflectances for use in the analysis were determined by:

$$\rho_i = \frac{V_i}{V_{ss(i)}} \times \rho_{ss(i)}$$

where

ρ_i = reflectance, channel i

V_i = voltage, channel i

$V_{ss(i)}$ = voltage, sun sensor, channel i

$\rho_{ss(i)}$ = reflectance, sun sensor, channel i

The constants shown above apply to the 3048 meter data collection altitude

and incorporate scanner characteristics.

Use of the red/blue channels for chlorophyll determination in the New York Bight restricted this measurement to the near surface. Calculations based on a 5 meter Secchi disc transparency indicate equivalent "blue" and "red" transparencies of approximately 2.8 meters and 2.3 meters, respectively.

The results of data processing for chlorophyll and transparency are shown in Figures 27 and 28. The ground-truth data (and times of collection) are indicated adjacent to the black squares in the figures. The results show a range in surface chlorophyll _a_ from 1.1 to 35 mg/m^3; and a Secchi disc transparency range from 4.6 meters to 1.1 meters.

Because of differences in time between ground-truth and remote sensing data collection, and uncertainties in station locations in the two data sets, validation of the remote sensing data is very difficult. The most suitable points of comparison are, (1) area near the tip of Sandy Hook and (2) ocean waters at the end of the run. The latter are outside of the waste dump areas and not as variable in terms of water quality as waters nearer to shore. Examining station V7 and ocean waters at the end of line 5, Figures 27 and 28; the calculated and ground truth results are as follows:

1. Chlorophyll _a_, Sta. V7

   $CHA = 10^{5.5668(.7031) - 2.4761}$

   $CHA = 27.4\ mg/m^3$

   Ground Truth: $22\ mg/m^3$

2. Chlorophyll _a_, end of line 5

   $CHA = 10^{5\text{-}5668(.5035) - 2.4761}$

   $CHA = 2.1\ mg/m^3$

   Ground Truth: $1.6\ mg/m^3$

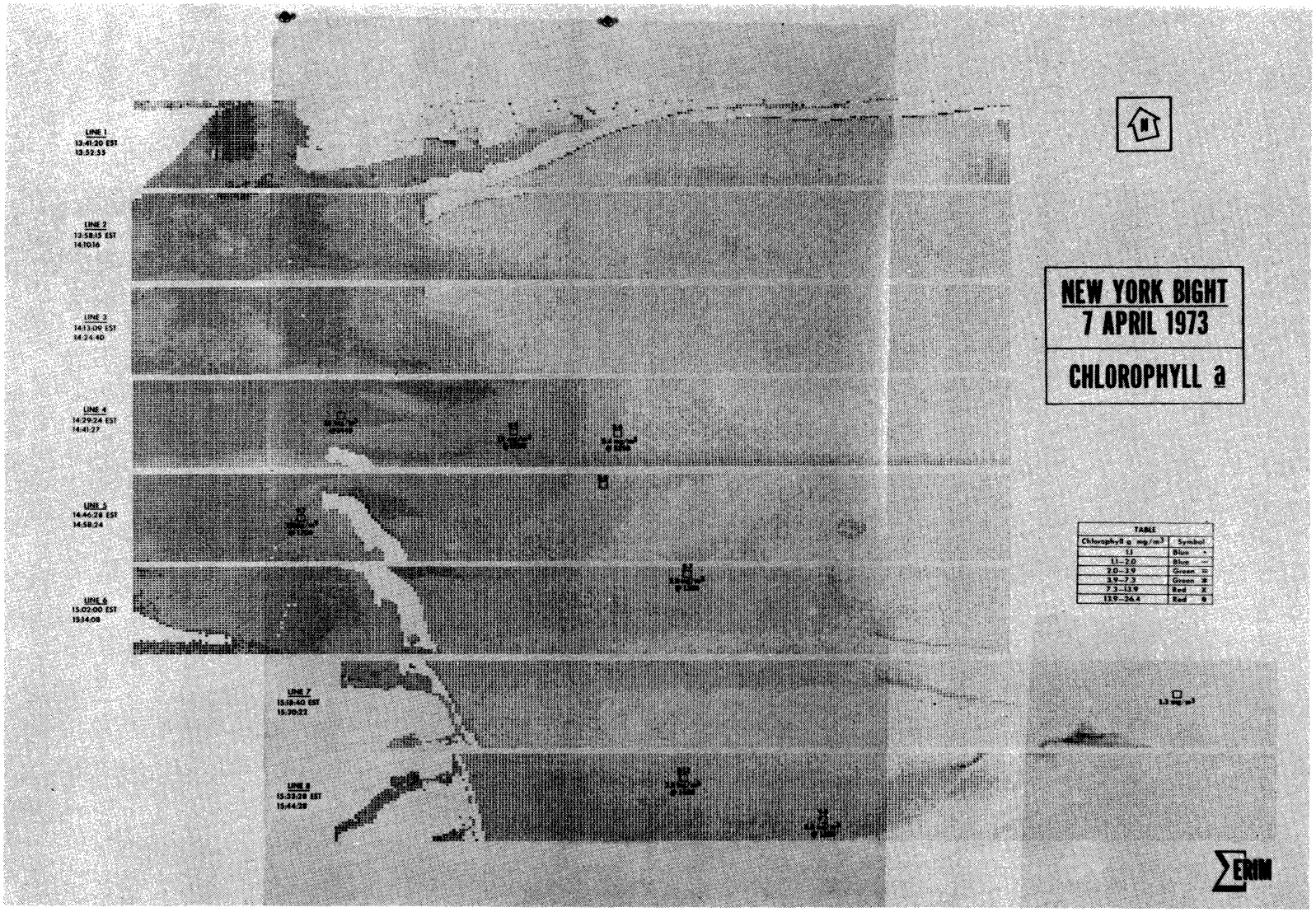

FIGURE 27. CHLOROPHYLL a, NEW YORK BIGHT, 7 APRIL 1973

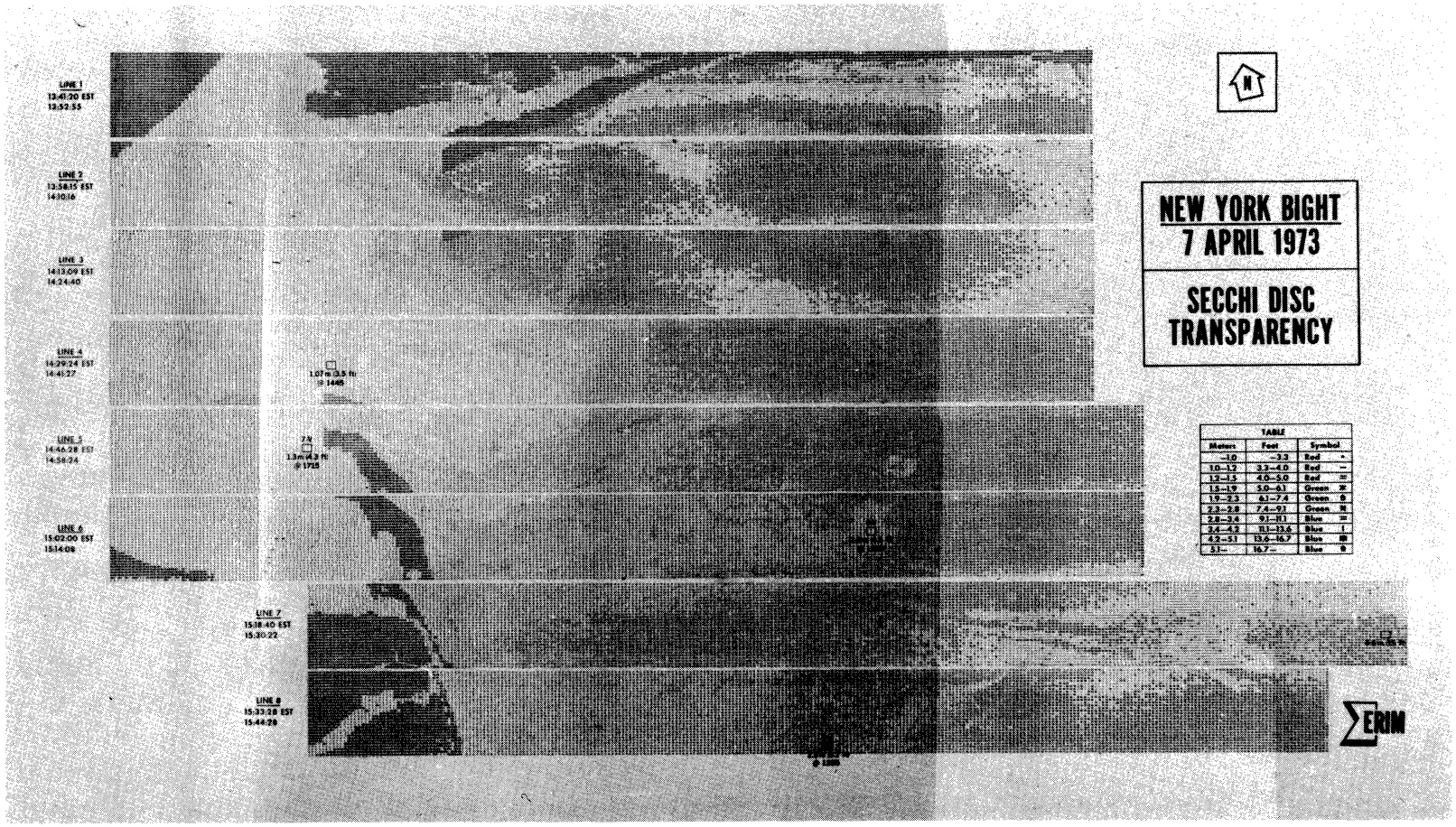

FIGURE 28. SECCHI DISC TRANSPARENCY, NEW YORK BIGHT, 7 APRIL 1973

3. Secchi Disc Transparency, Sta. V7

$T = 10^{0.8788(1.308) - 0.6235}$

$T = 3.4$ ft

Ground Truth: 4.3 ft

4. Secchi Disc Transparency, end of line 5

$T = 10^{0.8788(1.747) - 0.6235}$

$T = 8.2$ ft

Ground Truth: 10.0 ft

5. Secchi Disc Transparency, dump area, line 5-6

$T = 10^{0.8788(1.395) - 0.6235}$

$T = 4.0$ ft

Ground Truth = 4.3 ft

5.4 SECOND DERIVATIVE ANALYSIS

An initial analysis was performed to evaluate the potential of using the second derivative of the reflectance spectrum as an altitude independent technique for chlorophyll analysis. White [24] and Duntley [25] suggested analysis in the vicinity of 560 nm for chlorophyll determination.

The high and low chlorophyll locations shown in line 5, Figure 27, were used in the analysis. The numerical technique described in section 4.2 was implemented by a computer program and used to calculate the second derivatives. The results are shown in Figure 29. The solid line corresponds to a high chlorophyll content ($\pm$ 22 mg/m^3)whereas the dotted lines represent low chlorophyll content ($\pm$ 2 mg/m^3) at three different scan angles. At an altitude of 3048 meters, a scan angle of 40°-45° significantly increases path radiance.

The results of the initial analysis show a positive correlation between the second derivative at 545 nm and chlorophyll content, and a

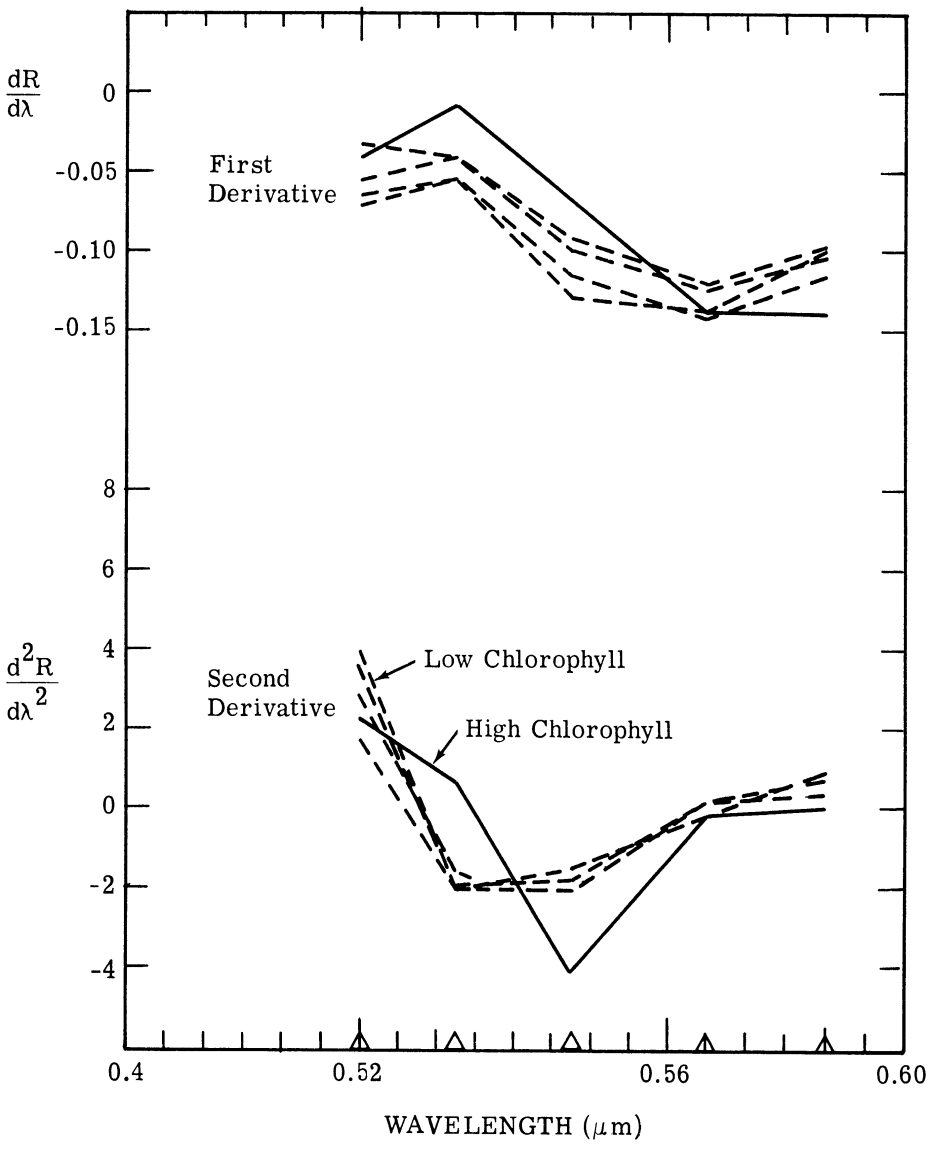

FIGURE 29. DERIVATIVE SPECTRA

negative correlation at 575 nm. The inflection point is located at approximately 560 nm. Furthermore, comparison of the first and second derivatives for the low chlorophyll curves indicate that path radiance effects are being eliminated, as indicated by theory.

Success in the use of the second derivative requires narrow spectral bands. The spectral bands used in the initial test were approximately 30 nm wide, as determiend at the 50% points. This is considerably wider than the 10 nm band widths which are desirable for second derivative analysis.

5.5 ERTS-1 DATA ANALYSIS

Processing of ERTS-1 data under this program was limited to an analysis of the bay areas west of Sandy Hook including Lower Bay, Raritan Bay, Sandy Hook Bay, and the lower portion of Upper Bay. The study area as seen by ERTS-1 on 7 April 1973 is shown in Figure 30.

Digital processing of ERTS-1 data was performed to differentiate water masses in terms of major suspended solids differences. The two digital maps produced are shown in Figures 31 and 32. The data values (grey levels) and standard deviations for the major target areas, derived from ERTS Computer Compatible Tapes (CCT's), are listed in Table 3. The values shown represent the "means" of approximately 100 resolution elements for each selected area. The "ocean" area in the table represents the relatively clean offshore waters away from waste-dump areas. Typical suspended solids concentrations in the "ocean" area are 4 mg/ℓ.

As indicated in Section 4.2.1 an introduction of particulates into a water column will result in an increased reflectance in the red spectral region. Prior experience has shown that MSS 5 (0.6-0.7 μm) is useful for

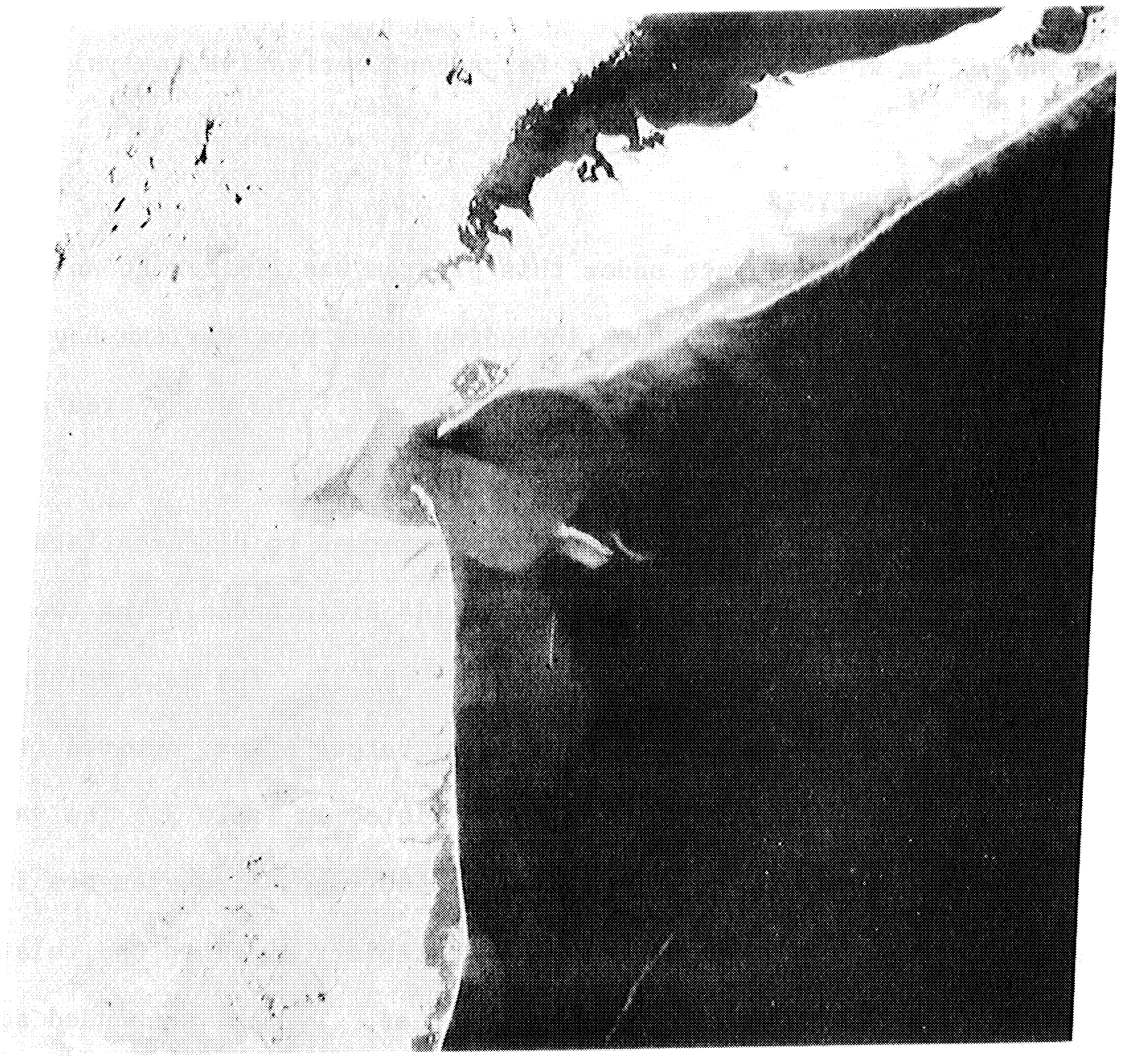

FIGURE 30. ERTS-1 DATA, NEW YORK BIGHT, 7 APRIL 1973.
MSS-5 (0.6-0.7 μm) E-1258-15082.

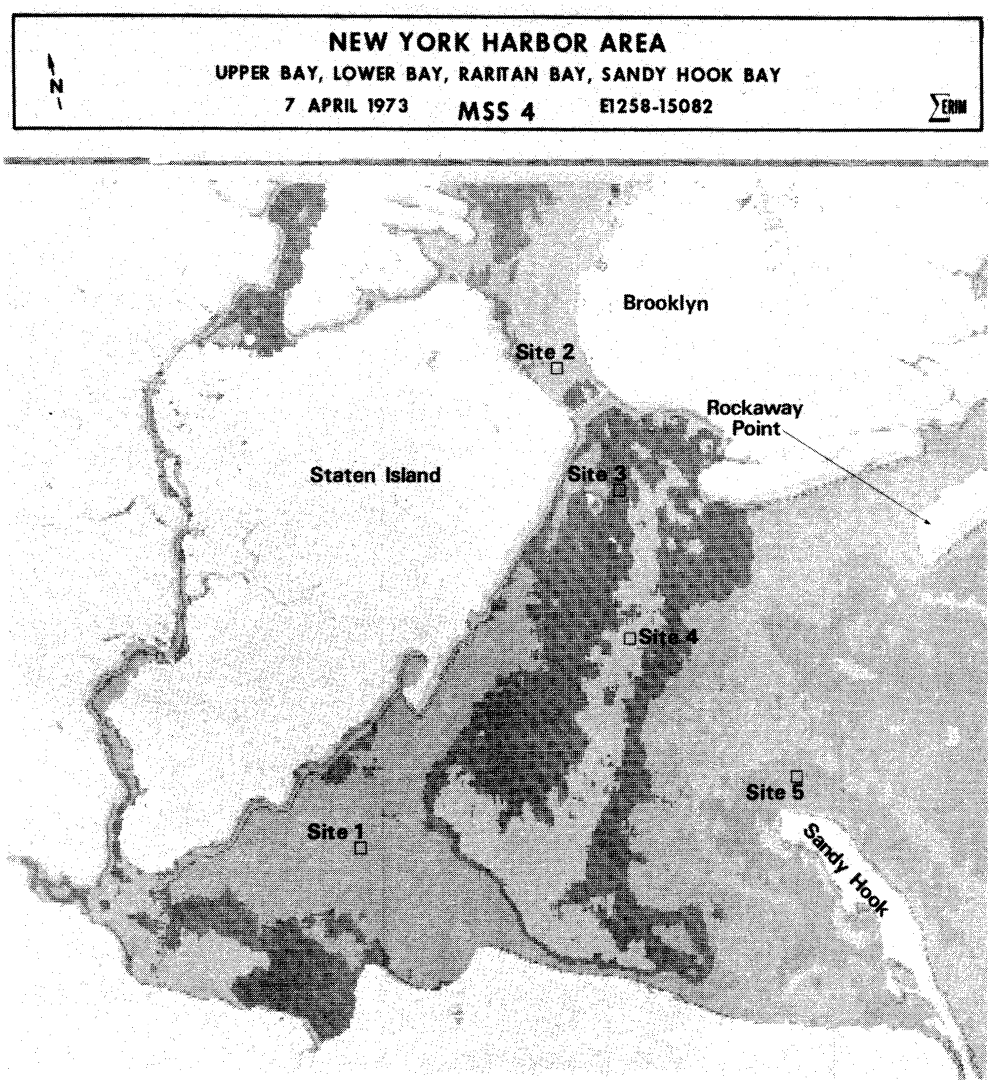

FIGURE 31. NEW YORK HARBOR AREA DIGITAL MAP, MSS-4

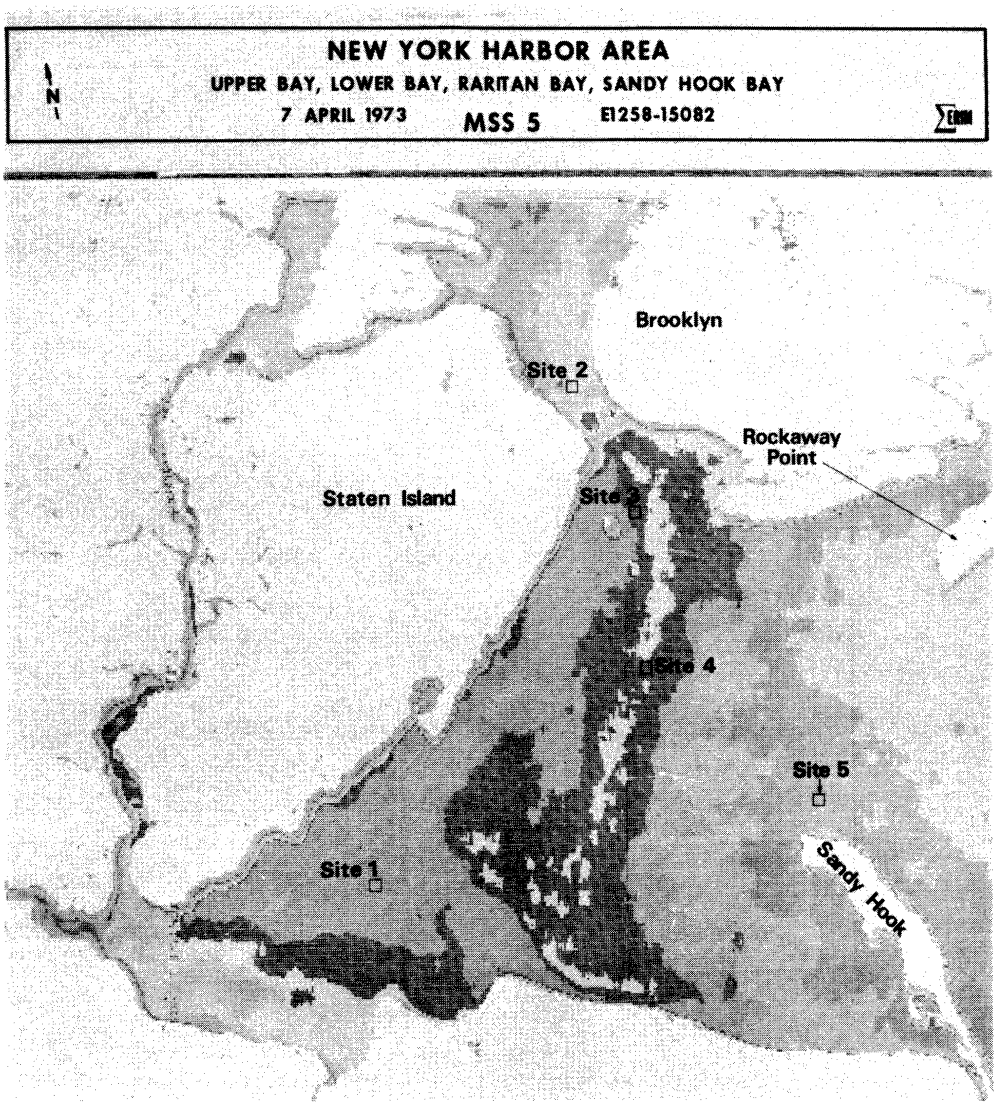

FIGURE 32. NEW YORK HARBOR AREA DIGITAL MAP, MSS-5

TABLE 3

CALCULATED SUSPENDED SOLIDS, NEW YORK HARBOR AREA
7 APRIL 1973, E 1258-15082

SITE	CHANNEL	DATA MEAN VALUE	STANDARD DEVIATION	CALCULATED SUSPENDED SOLIDS mg/ℓ
1	1	25.00	.00	16.6
	2	14.70	.46	
	3	7.79	.41	
	4	1.00	.61	
2	1	28.00	.00	50.5
	2	20.10	.30	
	3	10.12	.33	
	4	1.64	.66	
3	1	26.00	.00	22.2
	2	15.95	.22	
	3	8.00	.00	
	4	1.25	.59	
4	1	27.00	.00	23.0
	2	16.11	.32	
	3	8.00	.00	
	4	.98	.40	
5	1	23.00	.00	10.7
	2	13.00	.00	
	3	7.00	.00	
	4	1.00	.67	
OCEAN	1	19.82	.54	3.9
	2	9.79	.72	
	3	5.33	.67	
	4	0.87	.57	

determining suspended solids concentrations and related properties. The term suspended solids is defined as "total non-filtrable residue" as prescribed in Standard Methods [3]. Surface concentrations of suspended solids were calculated using the following empirical relationship;

$$C = 0.00116\ D^{3.55953}$$

where

C = mg/ℓ suspended solids

D = data value (grey level) MSS 5

The results are included in Table 3. Since ground-truth data in the bay area were not collected by ERIM and were not available from other sources, the applicability of the above equation is untested. Normally data from a pair of ground-truth stations representing the high and low concentrations anticipated are required for validation of the constants in the equation. Hence the values listed in Table 3 must be regarded as relative concentrations.

The scene depicted in Figures 31 and 32 illustrates an incoming tide condition, 36 minutes prior to high-water at Sandy Hook. As a consequence a ridge of relatively high suspended solids has developed near the center of the bay area.

The above brief analysis of ERTS-1 data is presented largely to demonstrate the potential of satellite remote sensing for providing data which can be used in the analysis of the movement of water masses in an estuarine situation.

6

CONCLUSIONS

Use of remote sensing, both aircraft and satellite, is demonstrated in studies of the highly complex and dynamic estuarine and coastal environment as represented by the New York Bight and adjacent bay areas. Interpretation and analysis of data collected by conventional point-sampling techniques is likely to be extremely difficult without reference to remote sensing data. The optimum solution is to exploit the capabilities of remote sensing technology and combine the information so derived with data acquired by conventional point-sampling methods. Therefore, the data and data products contained in this report are presented in the hope that they will be incorporated into the total environmental data base for the MESA program in the New York Bight.

The program of remote sensing data collection and analysis yielded information regarding surface temperature distribution, barge dumping of wastes, movement of water masses, transparency, and surface chlorophyll. The problem of chlorophyll determination is complex, and as a result no simple straight-forward solutions are possible. The empirical approach used in this analysis is intended solely for use in relatively productive waters such as those found in the New York Bight.

REFERENCES

1. P. G. Hasell, Jr., et al., "Michigan Experimental Multispectral Mapping System: A Description of the M7 Airborne Sensor and Its Performance," Report No. 190900-10-T, Environmental Research Institute of Michigan, Ann Arbor, January 1974.

2. D. K. Clark, J. B. Zaitzeff, L. V. Strees, and W. S. Glidden, "Computer Derived Coastal Water Classifications Via Spectral Signatures," Proceedings, Ninth International Symposium on Remote Sensing of Environment, Environmental Research Institute of Michigan, Ann Arbor, 15-19 April 1974, pp. 1213-1239.

3. Standard Methods for the Examination of Water and Wastewater, 13th Ed., A.P.H.A, New York, 1971.

4. Biological Field and Laboratory Methods, EPA 670/4-73-001, U. S. Environmental Protection Agency, National Environmental Research Center, Cincinnati, Ohio, July 1973.

5. J. N. Hamilton, J. A. Rowe, and D. Anding, "Atmospheric Transmission and Emission Program," Report No. TOR-0073 (3050-02)-3, The Aerospace Corp., El Segundo, California, 1973.

6. R. E. Turner, "Remote Sensing in Hazy Atmospheres," Proceedings of ACSM/ASP Meeting in Washington, D. C., March, 1972.

7. R. E. Turner, "Radiative Transfer in Model Atmospheres (Scattering)," Course Notes, Advanced Infrared Technology, The Ann Arbor Engineering Summer Conference, 1972.

8. R. E. Turner, "Radiative Transfer in Real Atmospheres," Report No. 190100-24-T, Environmental Research Institute of Michigan, Ann Arbor, 1974.

9. J. H. Ryther and C. S. Yentsch, "The Estimation of Phytoplankton Production in the Ocean From Chlorophyll and Light Data," Limnology and Oceanography, Vol. 2, pp. 281-286.

10. T. E. Bailey, "Measurement and Detection of Eutrophication," J. of the Sanitary Engineering Div., Am. Soc. Civil Eng., Vol. 93, 1967, pp. 121-132.

11. C. J. Lorenzen, "Surface Chlorophyll as an Index of the Depth, Chlorophyll Content, and Primary Productivity of the Euphotic Layer," Limnology and Oceanography, Vol. 15, 1970, pp. 479-480.

12. J.D.H. Strickland, "Measuring the Production of Marine Phytoplankton, Bulletin No. 122, Fisheries Res. Board of Canada, Ottawa, Ontario, 1960.

13. H.H. Seliger and W.D. McElroy, Light: Physical and Biological Action, Academic Press, New York, N.Y., 1965.

14. B.K. Gazey, "Visibility and Resolution in Turbid Waters," Underwater Science and Technology Journal, Vol. 2, 1970, pp. 105-115.

15. G. Suits, "Preliminary Results of Water Reflectance Calculations Using AQUACAN," Unpublished Memo, Environmental Research Institute of Michigan, Ann Arbor, January, 1973.

16. G. L. Clarke, G. C. Ewing, and C. J. Lorenzen, "Spectra of Backscattered Light from the Sea Obtained from Aircraft as a Measure of Chlorophyll Concentration," Science, Vol. 167, 1970, pp. 1119-1121.

17. J. C. Arvesen, E. C. Weaver, and J.P. Millard, "Rapid Assessment of Water Pollution by Airborne Measurement of Chlorophyll Content," Paper No. 71-1097, Proceedings, Am. Inst. of Aeronautics and Astronautics Joint Conference on Sensing of Environmental Pollutants, Palo Alto, California, November 1971.

18. K. Savastano, E. Pastula, G. Woods, and K. Faller, "Preliminary Results of Fisheries Investigation Associated with Skylab-3," Proceedings Ninth International Symposium on Remote Sensing of Environment, Environmental Research Institute of Michigan, Ann Arbor, 1974, pp. 1013-1042.

19. J. L. Mueller, "Remote Measurement of Chlorophyll Concentration and Secchi-Depth Using the Principal Components of the Ocean's Color Spectrum," Fourth Annual Earth Resources Program Review, NASA Manned Spacecraft Center, Houston, Texas, 4:105-1-105-13, 1972.

20. C. T. Wezernak, "The Use of Remote Sensing in Limnological Studies," Proceedings Ninth International Symposium on Remote Sensing of Environment, Environmental Research Institute of Michigan, Ann Arbor, Michigan, 1974, pp. 963-980.

21. S.Q. Duntley, W.H. Wilson, and C.F. Edgerton, "Detection of Ocean Chlorophyll from Earth Orbit, in Ocean Color Analysis," Technical Report SIO Ref. 74-10, Scripps Institution of Oceanography, University of California, San Diego, 1974, pp. 1-1 to 1-37.

22. G.E. Fogg, Algal Cultures and Phytoplankton Ecology, The University of Wisconsin Press, Madison, Wisconsin, 1966, 126 pp.

23. A.T. Giese and C.S. French, "The Analysis of Overlapping Spectral Absorption Bands by Derivative Spectrophotometry," Applied Spectroscopy, Vol. 9, 1955, pp. 78-96.

24. P.G. White, "A Technique for the Reduction and Analysis of Ocean Spectral Data," Fourth Annual Earth Resources Program Review, NASA Manned Spacecraft Center, Houston, Texas, 4:103-1-103-10, 1972.

25. S.Q. Duntley, "Optical Methods for Detection of Water Pollution," Proceedings of the Environmental Quality Sensor Workshop, at Western Environmental Research, Environmental Protection Agency, Washington, D.C., 30 November - 2 December 1971, pp. II-15 to II-27.

DISTRIBUTION LIST

National Oceanic and Atmospheric Administration
National Environmental Satellite Service
3737 Branch Avenue, Suite 405
Hillcrest Heights, Maryland 20031 (100)

Attention: D.K. Clark